

# Spectroscopic Calibrations for a Better Characterization of Stars and Planets

Guilherme Domingos  
Carvalho Teixeira

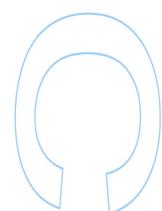
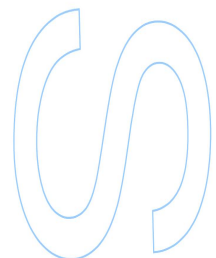
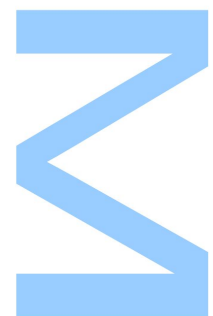
Mestrado em Astronomia  
Departamento de Física e Astronomia  
2014

**Orientador**

Sérgio A. G. Sousa,  
Professor Auxiliar Convidado, Faculdade de Ciências da Universidade do Porto

**Coorientador**

Mário João P. F. G. Monteiro,  
Professor Associado, Faculdade de Ciências da Universidade do Porto







Todas as correções determinadas pelo júri, e só essas, foram efetuadas.

O Presidente do Júri,

Porto, \_\_\_\_ / \_\_\_\_ / \_\_\_\_

**N**

S

Q





---

# Spectroscopic Calibrations for a Better Characterization of Stars and Planets

Master in Astronomy Dissertation

---

**Author:**

Guilherme Domingos Carvalho Teixeira<sup>1,2</sup>

**Supervisors:**

Sérgio A. G. Sousa<sup>1,2</sup> and Mário João P. F. G. Monteiro<sup>1,2</sup>

**Affiliations:**

<sup>1</sup>Centro de Astrofísica, Universidade do Porto, Rua das Estrelas, 4150-762 Porto, Portugal

<sup>2</sup>Departamento de Física e Astronomia, Faculdade de Ciências, Universidade do Porto, Rua do Campo Alegre,  
4169-007 Porto, Portugal



# Acknowledgements

The work leading to this dissertation was supported by a research fellowship (Ref: CAUP2013-05Unl-BI), funded by the European Commission through project SPACEINN (FP7-SPACE-2012-312844).

I would like to thank the guidance and support of both my supervisors during this work.

I would also like to thank Lisa Benamati for the help with the sample of 256 giant stars.

A special thanks to Maria Tsantaki for the valuable discussions, and for the help with some of the plots.

A very special acknowledgment goes to someone that must remain unnamed but who was, nevertheless, the most special person to me during this entire year. Thank you for the support, the friendship, the company, the good times, the bad times, the laughs, and the tears. These have been interesting times and I wouldn't change a single thing that happened. But, above all, thank you for always believing in me. I will never forget *you*. Thank you for everything.





# Abstract

The determination of precise and accurate stellar parameters has become one of the major challenges in current astrophysics. In particular, the amount of data currently being made available by large survey programs, like the GAIA-ESO survey makes the existence of quick methods for stellar parameter determination a necessity.

This project was aimed at the computation of a new spectroscopic calibration for quick effective temperature determinations for a wide range of stellar spectral types. This new calibration was accomplished by building upon existing techniques based on line-ratio relations.

We used spectra from three different stellar samples and homogeneously determined parameters in order to obtain the new temperature calibration. The new calibration is adequate for both FGK-dwarfs and GK-giant stars with parameters within the intervals:  $4500 \text{ K} < T_{\text{eff}} < 6500 \text{ K}$ ,  $2 < \log g < 4.9$ ,  $-0.8 < [\text{Fe}/\text{H}] < 0.5$ . There was a definite improvement of the new calibration with the standard deviation going from 112 K to 74 K for a sample composed of both giants and dwarfs.

We also successfully used two independent samples to test our new calibration. We have found that the new calibration produces results with a good agreement with the values from other methods if we consider only stars within the applicability range.

We have obtained new effective temperature values for the GES benchmark stars which will be used by the GES-CoRoT collaboration.

We have developed a new computational code, GeTCal, which can determine new calibrations given any stellar spectra and line-list as calibration samples. This code has been made available online.

The new calibration will be included in one of the ESPRESSO data analysis pipelines.

## Keywords

Stellar parameters, Spectroscopy, Line-Ratios, Temperature

## Resumo

A determinação de parâmetros estelares com precisão e exactidão tornou-se um dos maiores desafios da astrofísica recente. Em particular, a quantidade de dados que vão sendo tornados públicos por grandes programas de observação, tal como o programa GAIA-ESO, torna a existência de métodos rápidos para a determinação de parâmetros numa necessidade.

Este projecto foi focado na obtenção de uma nova calibração espectroscópica para determinações rápidas de temperatura para um conjunto alargado de classes espectrais estelares. Esta nova calibração foi conseguida utilizando técnicas existentes baseadas em relações entre rácios de linhas espectrais.

Utilizamos os espectros de três diferentes amostras de estrelas e parâmetros determinados de forma homogênea de modo a obter a nova calibração de temperatura. A nova calibração é adequada tanto para estrelas FGK-anãs como para estrelas GK-gigantes desde que estejam nos intervalos:  $4500 \text{ K} < T_{\text{eff}} < 6500 \text{ K}$ ,  $2 < \log g < 4.9$ ,  $-0.8 < [\text{Fe}/\text{H}] < 0.5$ . Houve uma melhoria definitiva na nova calibração, o desvio padrão passou de 112 K para 74 K para uma amostra de anãs e gigantes.

Também usamos com sucesso duas amostras independentes para testar a nossa nova calibração. Determinamos que a nova calibração produz resultados em concordância com os valores de outros métodos se considerarmos apenas as estrelas dentro do nosso intervalo de aplicabilidade.

Obtivemos novas temperaturas effectivas para estrelas standard do programa GES, os quais serão usados na colaboração GES-CoRoT

Desenvolvemos um novo código computacional, o GeTCal, o qual pode determinar novas calibrações dada uma qualquer amostra de calibração e lista de linhas espectrais. Este código foi disponibilizado online.

A nova calibração vai ser incluída num dos pipelines de análise de dados do ESPRESSO.

## Palavras chave

Parâmetros estelares, Espectroscopia, Razão entre linhas, Temperatura

# Contents

|          |   |           |
|----------|---|-----------|
| <b>1</b> | <b>Introduction</b>   | <b>21</b> |
| 1.1      | Methods for determining stellar parameters . . . . .        | 22        |
| 1.1.1    | 1.1.1 Photometry . . . . .                                  | 23        |
| 1.1.2    | 1.1.2 Spectroscopy . . . . .                                | 24        |
| 1.1.3    | 1.1.3 Line-ratios . . . . .                                 | 26        |
| <b>2</b> | <b>The ARES+MOOG method</b>                                 | <b>29</b> |
| 2.1      | ARES . . . . .  | 30        |
| 2.2      | MOOG . . . . .  | 34        |
| 2.2.1    | 2.2.1 Dependence on the effective temperature . . . . .     | 35        |
| 2.2.2    | 2.2.2 Surface Gravity dependence . . . . .                  | 35        |
| 2.2.3    | 2.2.3 Microturbulence . . . . .                             | 37        |
| 2.2.4    | 2.2.4 Minimization code . . . . .                           | 37        |
| <b>3</b> | <b>The TMCalc code</b>                                      | <b>39</b> |
| 3.1      | The calibration algorithm: GeTCal . . . . .                 | 42        |
| 3.2      | The New Calibration . . . . .                               | 46        |
| 3.2.1    | Re-derivation and calibration of the Sousa sample . . . . . | 46        |
| 3.2.2    | Application of the S+T-calibration . . . . .                | 47        |
| 3.2.3    | Obtaining the joint calibration . . . . .                   | 49        |
| <b>4</b> | <b>The new parameters</b>                                   | <b>53</b> |
| 4.1      | New parameter tables . . . . .                              | 53        |

|          |   |           |
|----------|---|-----------|
| 4.2      | An independent 56 giant-star sample . . . . .       | 55        |
| 4.3      | The GAIA-ESO survey benchmark star sample . . . . . | 56        |
| 4.4      | Limits of the new calibration . . . . .             | 58        |
| <b>5</b> | <b>Summary</b>                                      | <b>59</b> |
| 5.1      | Future Work . . . . .                               | 60        |
|          | <b>Bibliography</b>                                 | <b>61</b> |

# List of Figures

- 1.1 From Casagrande et al. (2010). Left upper panel: comparison between the observed HD 209458 CALSPEC spectrum (black line) and the synthetic spectra derived for two different  $T_{\text{eff}}$ , using an absolute calibration (blue line) and increasing the infrared absolute calibration by 5% (red line). Left lower panel: ratio of synthetic to observed spectra. Full circles are the ratio between the fluxes obtained once the Vega calibration is used with the observed magnitudes and the fluxes obtained directly from the convolution of the CALSPEC spectrum with the appropriate filter transmission curve. Error bars take into account uncertainty in the Vega calibration and zero points, as well as in the observed magnitudes. Right panel: reduced  $\chi^2$  for various  $T_{\text{eff}}$  solutions corresponding to different adopted absolute calibrations. The choice of Casagrande et al. (2010) always lies very close to the minima obtained fitting a parabola to the data (lines of different style). Different symbols correspond to cut longward of  $0.66 \mu\text{m}$  (diamonds),  $0.82 \mu\text{m}$  (squares) and  $1.46 \mu\text{m}$  (triangles) as explained in Casagrande et al. (2010). The sigma levels have been computed using the incomplete gamma function for the number of degrees of freedom longward of our cuts. . . . . 23
- 1.2 An example of the spectral synthesis method for the sun. The synthetic spectra is the blue line, the black line is the observed spectra. The dark areas are the line points recognized by the code while the pink areas are the continuum points. This plot was obtained using the Spectroscopy Made Easy (SME), version 3.3 software (Valenti & Piskunov 1996). . . . . 25
- 1.3 Diagram that presents the definition of Equivalent Width(EW). It is the width of a rectangle centered on a spectral line and which has the same area as the line. . . . . 26

|     |   |    |
|-----|---|----|
| 1.4 | From Tsantaki et al. (2014). Solar absorption lines(solid line), broadened by $v \sin i$ 10 km/s (pink), $v \sin i$ 15 km/s(blue) and 20 km/s(red). Blending at these rates due to rotation makes the determination of EW harder. . . . .   | 27 |
| 1.5 | From Desidera et al. (2011). Effective temperature with ARES on solar spectra artificially broadened to various values of $v \sin i$ . Up to values of $v \sin i$ of 18 km/s results are robust. . . . .  | 28 |
| 2.1 | Flowchart detailing the ARES+MOOG method (Sousa 2013). See the text for details. .  | 30 |
| 2.2 | From Sousa et al. (2007). A synthetic spectrum region with a signal-to-noise ratio around 50. The filled line represents the fit to the local continuum through a 2nd-order polynomial based on the points that are marked as crosses in the spectrum. The variations induced by different values of the parameter $rejt$ are readily visible. . . . .  | 32 |
| 2.3 | From Sousa (2013). Abundance of FeI as a function of excitation potential (E.P. ) and reduced wavelength (R. W.). The top panel shows the result for the correct stellar parameters while in the bottom panels the temperature was changed to a lower value (5600K) - left panel, and an upper value (5900K) - right panel. . . . .   | 36 |
| 3.1 | From Sousa et al. (2012). In the top panel, the comparison between the effective temperatures derived from the ARES+MOOG method and the ones derived using TMCalc for the calibration sample of Sousa et al. (2010). In the bottom plot, a similar plot is shown but for the sample of stars of Sousa et al. (2010), a sample independent of the calibration. Both panels also show the mean difference and the standard deviation for the comparisons. . . . . | 41 |
| 3.2 | Flowchart of the calibration algorithm GeTCal. The boxes represent files, the losangles represent subroutines and the elipses represent data stored in memory. . . . .  | 42 |
| 3.3 | Plot of the 3rd degree polynomial fit for the ratio between the lines: SiI(6142.49 Å) and TiI (6126.22 Å). The dashed lines represent the 2-sigma of the fit. The black dots represent the stars removed using the $2 - \sigma$ cut. Also shown is the error of the fit which is $82K$ . .  | 44 |



- 3.4 Plot of the fits for the ratio, the inverse of the ratio and the logarithm of the ratio between lines FeI 6739.52 Å and FeI 6793.26 Å, respectively from left to right. The blue lines are the linear fit, the green lines are the 3rd degree polynomial fit. The P\_sigma is the error of the 3rd degree polynomial fit, L\_sigma is the error of the linear fit and STARS is the number of stars used for the fit. In this case the polynomial of the inverse of the ratio was chosen as it had the lowest error,  $\sim 89K$ . . . . . 45
- 3.5 Comparison between the  $T_{\text{eff}}$  obtained using TMCalc and the  $T_{\text{eff}}$  obtained using the ARES+MOOG method for the sample of 451-FGK dwarf stars. The red circles are the results obtained for the original calibration, the blue open squares are the values using the new S+T calibration. The black line represents the identity line. A clear improvement can be seen for cool stars and for hot stars. . . . . 48
- 3.6 Comparison between the  $T_{\text{eff}}$  obtained using TMCalc and the  $T_{\text{eff}}$  obtained using the ARES+MOOG method for the sample of 256 giant stars. The red circles are the results obtained for the S+T-calibration, the blue open squares are the values using the new B calibration. The black line represents the identity line. A clear improvement can be observed. . . . . 49
- 3.7 Comparison between the  $T_{\text{eff}}$  obtained using TMCalc and the  $T_{\text{eff}}$  obtained using the ARES+MOOG method for the sample of the 451 FGK-dwarfs. The red circles are the results obtained using the S+T-calibration, the blue open squares are the values using the B-calibration. The black line represents the identity line. A clear deviation from linearity is observed using the B-calibration. . . . . 50
- 3.8 Comparison between the  $T_{\text{eff}}$  obtained using TMCalc and the  $T_{\text{eff}}$  obtained using the ARES+MOOG method for a sample composed by the 451 FGK-dwarfs and the Alves-sample of giants. The red circles are the results obtained using the S+T-calibration, the blue open squares are the values using the J-calibration. The black line represents the identity line. The J-calibration is able to compute the temperatures for both type of stars. 51
- 4.1 Comparison between the  $T_{\text{eff}}$  obtained using TMCalc and the  $T_{\text{eff}}$  obtained using the ARES+MOOG method for the sample of 56 giant stars used. The black line represents the identity line. . . . . 55

4.2 Comparison between the  $T_{\text{eff}}$  obtained using TMCalc and the  $T_{\text{eff}}$  obtained using the ARES+MOOG method for the COROT benchmark stars. The black line represents the identity line. . . . . 57

4.3 Comparison between the  $T_{\text{eff}}$  obtained using TMCalc and the  $T_{\text{eff}}$  obtained using the ARES+MOOG method for all stars used during our study. The black line represents the identity line. The colour code shows the value of  $\log g$  of each star. It is clear that most outliers are stars with very low  $\log g$  values. . . . . 58

# List of Tables

|     |  |    |
|-----|--|----|
| 3.1 | Difference between the $T_{\text{eff}}$ from the ARES+MOOG and TMCalc methods. . . . . | 48 |
| 3.2 | Summary of each calibration file used. . . . .   | 51 |
| 4.1 | Parameters for the Sousa-sample of FGK-dwarf stars, sample table. . . . .              | 54 |
| 4.2 | Parameters for the Alves-sample of GK-giant stars, sample table. . . . .               | 54 |
| 4.3 | Parameters for the independent 56 giant stars, sample table. . . . .                   | 56 |
| 4.4 | Parameters for the COROT benchmark stars, sample table. . . . .                        | 57 |
| 4.5 | Limits of applicability of the J-calibration. . . . .                                  | 58 |



# Chapter 1.

## Introduction

One of the main challenges in our current understanding of stellar astrophysics is how to derive accurate stellar parameters. Although fundamental parameters such as mass, and age are of the utmost importance to stellar studies, they are observationally impossible to obtain by any direct method. As such, the determination of these fundamental parameters depends entirely on the precision with which we can directly measure stellar atmospheric parameters. Stellar atmospheric parameters, such as effective temperature,  $T_{\text{eff}}$ , surface gravity,  $\log g$ , and metallicity,  $[\text{Fe}/\text{H}]$ , are basic properties that can be obtained through spectroscopic and/or photometric analysis, e.g. Sousa et al. (2007, 2010), Casagrande et al. (2010), Tsantaki et al. (2013).

The relevance of properly determining stellar parameters cannot be understated. Presently, stellar parameters have assumed an increased importance in lines of research such as studies of planet-host stars, galactic population studies, among others (Casagrande et al. 2010).

Studies of planet-host stars use stellar parameters to explore possible correlations between the parameters of the host-star and the presence of planets, and with the characteristics of the planets themselves, hopefully leading to the improvement of current planet-formation theories (Santos et al. 2004, Mortier et al. 2013, Tsantaki et al. 2014). Even a more fundamental use for stellar parameters is that they are essential to the determination of planetary mass and radius. Meanwhile, some recent galactic population studies have been focusing on how the galactic birth place may relate to stellar properties (Adibekyan et al. 2014).

Since the formation of spectral lines is conditioned by the stellar atmospheric properties, spec-

troscopy can help to unveil a wealth of information about the star itself.

Spectral lines act like tracers of elements and molecules present in stellar atmospheres as each wavelength is unique to a single transition of states of an element or molecule. Spectral lines, both in absorption and in emission can be formed by a variety of mechanisms, our work concerns those which are formed by the absorption of photons following the jump of an electron from one atomic level to another (Gray 2005).

The amount of absorbed light depends on the abundance of each given element, on the number of electrons present in each atomic energy level, and the element itself. Element abundance and the number of electrons in each energy level are severely influenced by the conditions of the stellar atmosphere such as  $T_{\text{eff}}$ ,  $\log g$ , and also microturbulent velocity,  $v_{\text{mic}}$  (Gray 2005).

Therefore, one can extrapolate the abundance of each element in a stellar atmosphere if the strength of each spectral line present in the spectra is measured and these atmospheric parameters are known.

In the last decades, there has been an emergence of a number of methods that determine stellar parameters from spectroscopy. One of the problems with most of these methods is that they are, usually, computational- and time-consuming. As such, a need for tools capable of correctly and quickly estimating these atmospheric parameters or, at least, some of them, has become a pressing concern (Sousa et al. 2012).

The main problem associated with building such general-purpose tools is tied with the fact that stars of different spectral types present different spectral features formed by the different atmospheric characteristics which characterize each stellar type. Therefore, any generalized method must be able to take these different characteristics into account and, as such, be calibrated in a way that reflects the inherent differences of spectral type.

## 1.1 METHODS FOR DETERMINING STELLAR PARAMETERS

There are a plethora of methods to determine stellar parameters but they can be grouped into two main categories of techniques: photometry and spectroscopy. Each of these categories has advantages and disadvantages that should be weighed in order to choose the method that better suits the

desired scientific goal.

### 1.1.1 Photometry

There are several photometry-based techniques to determine stellar parameters. Most of them are plagued by similar problems: dependency on the accuracy of the atmospheric models, reliance on the correct determination of the angular diameter of the star, reddening effects, uncertainties in the determination of stellar fluxes, just to name a few.

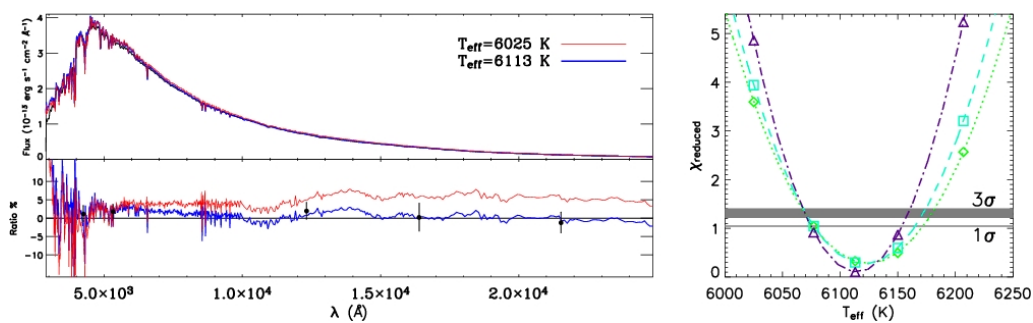


**Figure 1.1:** From Casagrande et al. (2010). Left upper panel: comparison between the observed HD 209458 CALSPEC spectrum (black line) and the synthetic spectra derived for two different  $T_{\text{eff}}$ , using an absolute calibration (blue line) and increasing the infrared absolute calibration by 5% (red line). Left lower panel: ratio of synthetic to observed spectra. Full circles are the ratio between the fluxes obtained once the Vega calibration is used with the observed magnitudes and the fluxes obtained directly from the convolution of the CALSPEC spectrum with the appropriate filter transmission curve. Error bars take into account uncertainty in the Vega calibration and zero points, as well as in the observed magnitudes. Right panel: reduced  $\chi^2$  for various  $T_{\text{eff}}$  solutions corresponding to different adopted absolute calibrations. The choice of Casagrande et al. (2010) always lies very close to the minima obtained fitting a parabola to the data (lines of different style). Different symbols correspond to cut longward of  $0.66 \mu\text{m}$  (diamonds),  $0.82 \mu\text{m}$  (squares) and  $1.46 \mu\text{m}$  (triangles) as explained in Casagrande et al. (2010). The sigma levels have been computed using the incomplete gamma function for the number of degrees of freedom longward of our cuts..

Our brief summary of a photometric method will be focused on a method which is considered to be one of the most reliable and used photometric methods, the infra-red flux method, hereafter IRFM. The reason for the increased usage of IRFM is linked to the fact that this method has a small dependency on models and is particularly suited for the determination the  $T_{\text{eff}}$  of F, G and K stars (Casagrande et al. 2010, Sousa et al. 2008).

The basis of the IRFM relies on the fact that the monochromatic infrared flux depends only on the first power of  $T_{\text{eff}}$ . On the contrary, the integrated flux is strongly dependent on the temperature,  $T_{\text{eff}}^4$ . The IRFM has a small dependency on other stellar parameters, like  $\log g$  and  $[M/H]$ , which are required to interpolate atmospheric models on a grid (Casagrande et al. 2010).

The IRFM evaluates the ratio between the bolometric flux,  $F_{\text{bol}}$ , and the monochromatic flux at a given infrared wavelength,  $F(\lambda_{\text{IR}})$ , as measured from the surface of the earth. Consequently, this ratio

is used as a tracer for  $T_{\text{eff}}$  (Casagrande et al. 2010).

Given that  $T_{\text{eff}}$  plays a very important role on the determination of stellar abundances, the IRFM, which provides an accurate and mostly model-independent method to determine  $T_{\text{eff}}$ , has been used with increasing frequency (Casagrande et al. 2010).

Another reason for the increased usage of the IRFM over the last few years was the advent of infrared surveys, like 2MASS. Since the IRFM requires infrared photometry, the appearance of homogeneous and all-sky surveys like 2MASS, allowed for the implementation of the IRFM on multiple stars and, consequently, the determination of colour-temperature relations (González Hernández et al. 2009). The temperatures obtained using the IRFM are frequently considered as benchmark values. Its only caveat is that, in spite of the high accuracy it consistently produces, and the fact that its results are free from non-LTE and granulation effects, both the adopted reddening and the absolute flux calibration can induce systematic errors in the results (González Hernández et al. 2009, Casagrande et al. 2010).

### 1.1.2 Spectroscopy

There are several spectroscopic techniques for stellar parameter determination. Some of those techniques rely on the intensity of each spectral line while others rely on the value of the equivalent width(EW) of each line.

Spectral synthesis methods rely on the production of synthetic spectra and fitting it to observations. The synthetic spectra is computed using different stellar atmospheric parameters and abundances and then, using a minimization code, fitting it to observations. Figure 1.2 shows the fit of a part of such a synthetic spectra to the observed spectra of the sun. These methods are, however, time consuming and their dependence on observed parameters introduces systematic errors that can only be mitigated using an uniform analysis (Tsantaki et al. 2014).

The TMCalc code and the ARES+MOOG methods which were used during this work are, in essence, EW methods. For this reason, we will present a short summary of the steps that are the foundation for all EW methods.

Before explaining the EW methods it is important to first present the definition of what is a EW. The EW of a spectral line is, essentially, a way to measure the area of the spectral line on a normalized intensity versus wavelength plot. It is defined as the width of a rectangle centered on a spectral line



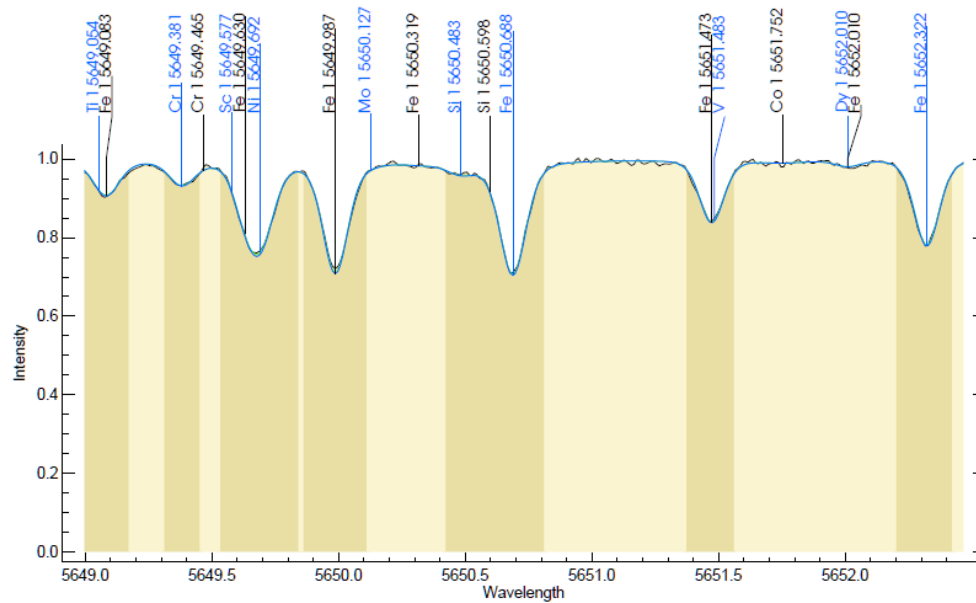


**Figure 1.2:** An example of the spectral synthesis method for the sun. The synthetic spectra is the blue line, the black line is the observed spectra. The dark areas are the line points recognized by the code while the pink areas are the continuum points. This plot was obtained using the Spectroscopy Made Easy (SME), version 3.3 software (Valenti & Piskunov 1996).

and which has the same area as the line in a normalized spectrum, a visual representation of an EW is shown in figure 1.3. The EW of a line is a measure of the strength of a given spectral line, with the obvious advantage that its value does not depend on the shape of the line, only on the method used to measure the area, making the EW more or less immune to effects such as line broadening. In certain conditions, and assuming local thermodynamical equilibrium (LTE), the EW of a line can be used to obtain the number of emitting or absorbing atoms (Carroll et al. 2006).

Any EW method can easily be summarized by the following steps:

1. A list of absorption lines with the corresponding atomic data is selected for the analysis for several elements;
2. A line-by-line analysis of the observational spectrum is performed and the EWs are measured independently;
3. Given the correspondent atmospheric parameters a stellar atmospheric model is adopted;
4. The measured lines and the atmospheric models are used to compute the individual line abundances;
5. The spectroscopic parameters are found once the excitation and ionization balance are valid

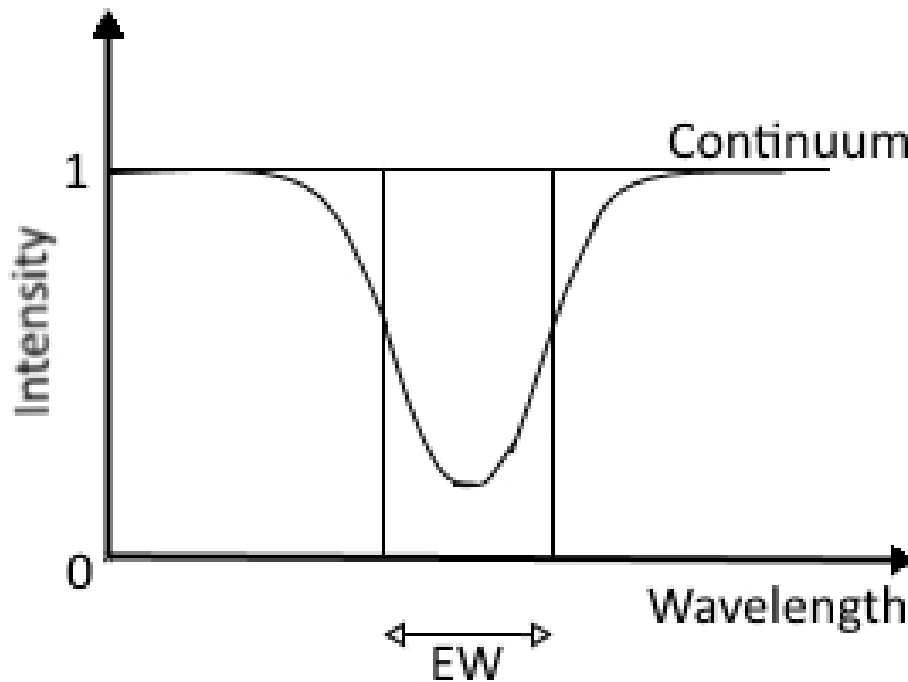


**Figure 1.3:** Diagram that presents the definition of Equivalent Width(EW). It is the width of a rectangle centered on a spectral line and which has the same area as the line.

for all the analyzed individual lines (see chapter 2), otherwise the process iterates from point 3 adopting new parameters;

The EW-based methods that can be found in literature usually differ in one or several of the following points: the choice of line-list, the choice of atmospheric models, and the computational code used to perform the steps described above (Sousa 2013).

### 1.1.3 Line-ratios

The use of line-ratios as a way to find the effective temperature of a star is deeply connected with the use of metal lines in a manner quite similar to finding out the spectral type of a star. Spectral lines of metals have varying sensitivities to  $T_{\text{eff}}$ . It is important to note that the origin of weak metal lines takes place, essentially, in the same photospheric layer which forms the continuum. EWs can be used for  $T_{\text{eff}}$  determinations but EW values can be greatly enhanced by factors such as microturbulence and other mechanisms. Of course, this leads to the preferred use of weak lines but these lines are difficult to measure and can be easily distorted by line blends (Gray 2005).

In order to solve some of the problems of  $T_{\text{eff}}$  determination from EW it is possible to use line-ratios.

The basic principle in this use is that using the ratio of two lines, preferably of the same element, we can dispense with factors such as abundance dependence. There is another interesting property of line ratios which is, if the lines used are close together, any errors associated the determination of the continuum will be greatly minimized. Also, if the lines are of similar strength, there is a compensation to the first order of macroturbulent broadening and chemical composition (Gray 2005).

Previous studies have shown that line-ratio calibrations can be used to return good estimates of temperatures, even for solar-type stars, up to relatively high rotation rates, up to 18 km/s (Sousa et al. 2010, Desidera et al. 2011). This limit is inexorably connected with the blending effect present at high rotation rates as shown in figure 1.4. It is also quite present in the larger inaccuracy in temperature determination patent in figure 1.5 which shows how temperature determination gets increasingly worse with rotation. This figure also shows us that lower resolution spectra will result in higher errors and larger uncertainties. The limit 18 km/s exceeds the capacity of typical EW methods due, in part, to the increase in the number of blends in higher rotation stars. In contrast, it has been recently shown that methods relying on synthesis for  $T_{\text{eff}}$  determination work well into the regime of fast-rotators, up to 50 km/s (Tsantaki et al. 2014), and are also effective with lower resolution spectra.

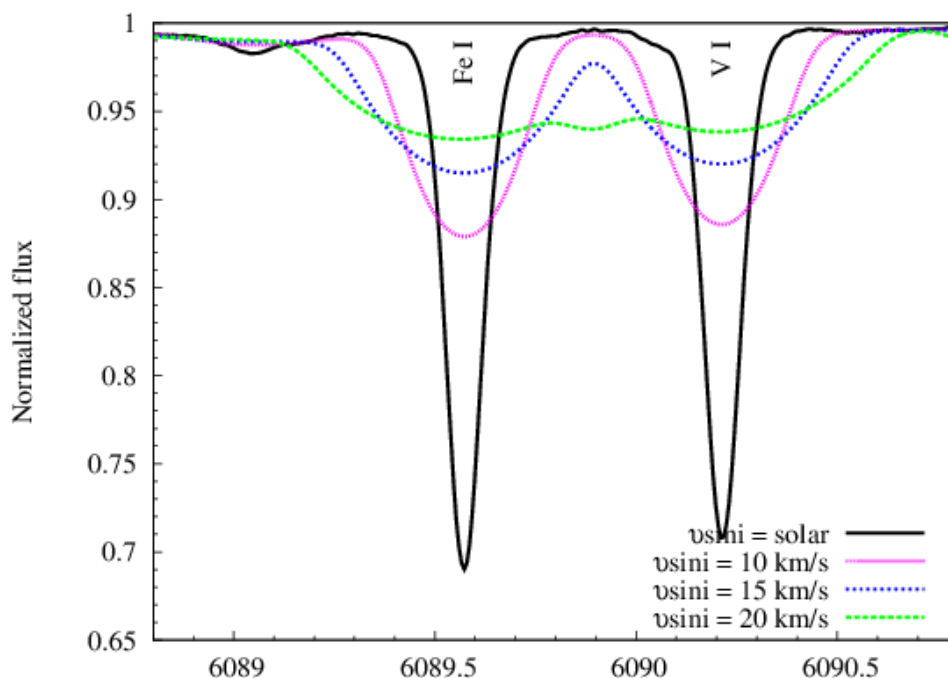


**Figure 1.4:** From Tsantaki et al. (2014). Solar absorption lines (solid line), broadened by  $v \sin i$  10 km/s (pink),  $v \sin i$  15 km/s (blue) and 20 km/s (red). Blending at these rates due to rotation makes the determination of EW harder.

The line-ratio calibrations made are based on weak metal lines all of which depend mainly on tem-

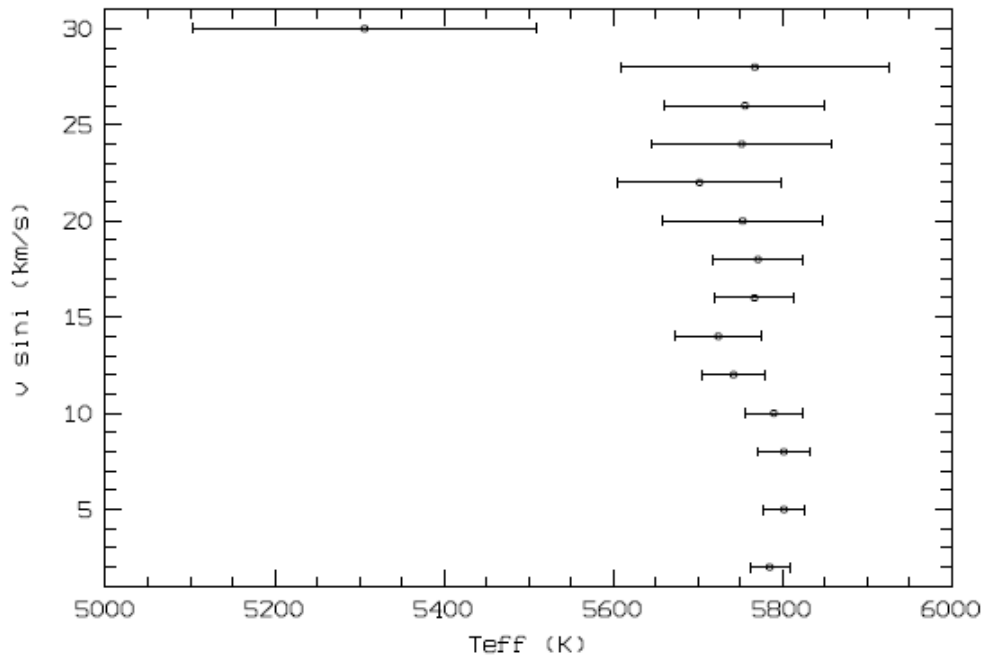


**Figure 1.5:** From Desidera et al. (2011). Effective temperature with ARES on solar spectra artificially broadened to various values of  $v \sin i$ . Up to values of  $v \sin i$  of 18 km/s results are robust.

perature. These lines are also less dependent on other parameters such as surface gravity and micro-turbulence. Most of metals on stellar atmospheres of sun-like stars are ionized so, changes in surface gravity will have a small impact in the abundance of neutral metals (Gray 2005, 1994, Kovtyukh et al. 2003). On the other hand, since we are dealing with weak lines any effect that microturbulence could have, which is noticeable in the wings of saturated lines, is also almost non-existent.

In order to choose line-ratios which have the required dependence on temperature and are independent of  $\log g$  and  $v_{\text{mic}}$ , the line-ratios have to fulfill important conditions: the distance between the lines in the denominator and the numerator should be small, they should have an excitation potential difference larger than 3 eV, and they should have the same ionization state. The distance condition is a way to restrict the line-ratios to lines lying close together in the wavelength domain and, therefore, avoid adverse effects that could arise from a poor continuum determination. The excitation potential condition, on the other hand, works as a way to limit line-ratios to those that are more sensible to temperature variations, since lines with higher excitation potential change faster with temperature (Sousa et al. 2010).

## Chapter 2.

### The ARES+MOOG method

During the course of this dissertation project we used a method based on the EW of spectral lines, this method is known as the ARES+MOOG method. The ARES+MOOG method, like other EW methods, first determines the strength of selected and well-defined absorption lines, assumes a certain atmospheric model, and translates the values into individual line abundances. A comparison is subsequently performed between the computed abundances and the theoretical predictions in order to obtain the correct parameters (Sousa 2013).

The ARES+MOOG method uses two software programs: ARES, an automatic code that measures EWs, and MOOG, a spectral analysis and synthesis software tool.

Figure 2.1 shows a flowchart that describes the ARES+MOOG method with some detail. First the spectrum and line-list are used with the ARES code to obtain the EW. Then the MOOG code is used to produce an atmospheric model, a minimization code is applied using the Downhill Simplex Method and in the end of this minimization code the stellar parameters are obtained (Sousa 2013).

Like other EW methods, one of the most crucial points of the method is the selection of lines to use. The choice of the lines will determine the accuracy and precision of the final results. As referred above, different EW methods use different line-lists. Line-lists with a large number of lines are able to produce statistically confident derived parameters. While, on the other hand, line-lists with a reduced number of lines usually have only well-known lines, which are well adapted for a specific type of stars, e.g. giants.

Another important factor of any EW method, including the ARES+MOOG method, is the adopted atomic data of the selected lines. Although values for the rest wavelengths and excitation potentials for

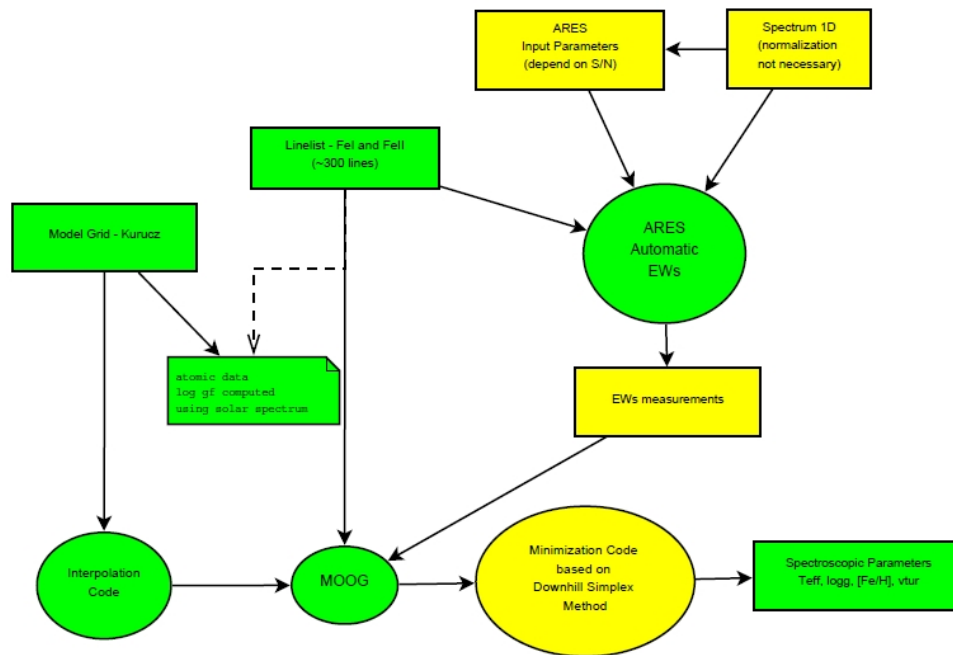


**Figure 2.1:** Flowchart detailing the ARES+MOOG method (Sousa 2013). See the text for details.

the lines can be considered to be consistent, the oscillator strengths,  $\log gf$ , are not precise between different line datasets. These laboratory values present large uncertainties that propagate and affect both the precision and accuracy of the derived stellar parameters (Sousa 2013).

The determination of elemental abundances is achieved by combining the effect of all the referred stellar atmospheric parameters,  $T_{\text{eff}}$ ,  $\log g$ ,  $v_{\text{mic}}$ , and  $[\text{Fe}/\text{H}]$ .

## 2.1 ARES

The abbreviation ARES stands for Automatic Routine for line Equivalent widths in stellar Spectra. As the name indicates, it is an automatic code that measures the EWs of the selected absorption lines in an input spectra (Sousa et al. 2007).

The approach taken by ARES is to have an estimation of the continuum position and determine the number of lines (in the case of blending) required for the best fit solution to the normalized spectrum around the selected line (Sousa et al. 2007).

ARES takes as input an one-dimensional spectrum, a list of spectral lines to measure and a file containing the parameters necessary for the computation of EWs. The code proceeds to select a region neighbouring the line, sets the continuum position and identifies the number and position of the

lines, each line fitted to a Gaussian profile, required to fit the local spectrum. The parameters of each fit are used to calculate the value of the EW of each line. The resulting values are then produced into a user-defined file (Sousa et al. 2007, Sousa 2013).

In order to successfully execute ARES a series of input parameters are required. Among these parameters are: the input spectra 1D-fits filename, the line-list, the output filename, the wavelength domain to be used, the minimum interval between successive lines, the wavelength interval to be considered around each line, the minimum value accepted for the EW, the calibration parameters for the continuum determination and noise control, and the display parameters. It is important to note that the input spectrum must have already been reduced and corrected for the Doppler-shift (Sousa et al. 2007, Sousa 2013).

The computation of each EW is done locally around each line, as noted above, with this parameter space being defined by the user input parameters. The continuum will, consequently, be obtained iteratively by choosing points above the fit of a second order polynomial function multiplied by a value defined by the user input parameter *rejt*. The *rejt* parameter is crucial in order to deal with the S/N of the spectra. Each spectra used had a predetermined S/N which was then used to determine the value of the *rejt* parameter, which was defined according to the table shown in Mortier et al. (2013).

The impact that changes in the *rejt* parameter can have on the measurement of the EW of a line is presented in figure 2.2. When working with spectra with higher values of S/N this parameter should be closer to 1. Again, it is important to stress that the input spectrum should be reduced, calibrated in wavelength, without cosmic rays and normalized (Sousa et al. 2007).

In order to find the peaks of the lines ARES uses the well-known properties of derivatives of a function and computes the first three derivatives of each line profile (Sousa et al. 2007).

Another problem which is addressed by ARES is overcoming the problem of noise. In order to do that, ARES applies a numerical smoothing to the array of the derivatives and reduces some of the noise. An additional input parameter, *smoothder*, is important since it takes into account the numerical resolution of the spectra (Sousa et al. 2007, Sousa 2013).

Considering that with a noise value high enough, the procedure could, in principle, mistakenly identify lines that are close to one another but which are in reality the same line, an additional parameter of ARES, *lineresol* can be used to deal with this, the parameter sets the allowed minimal distance

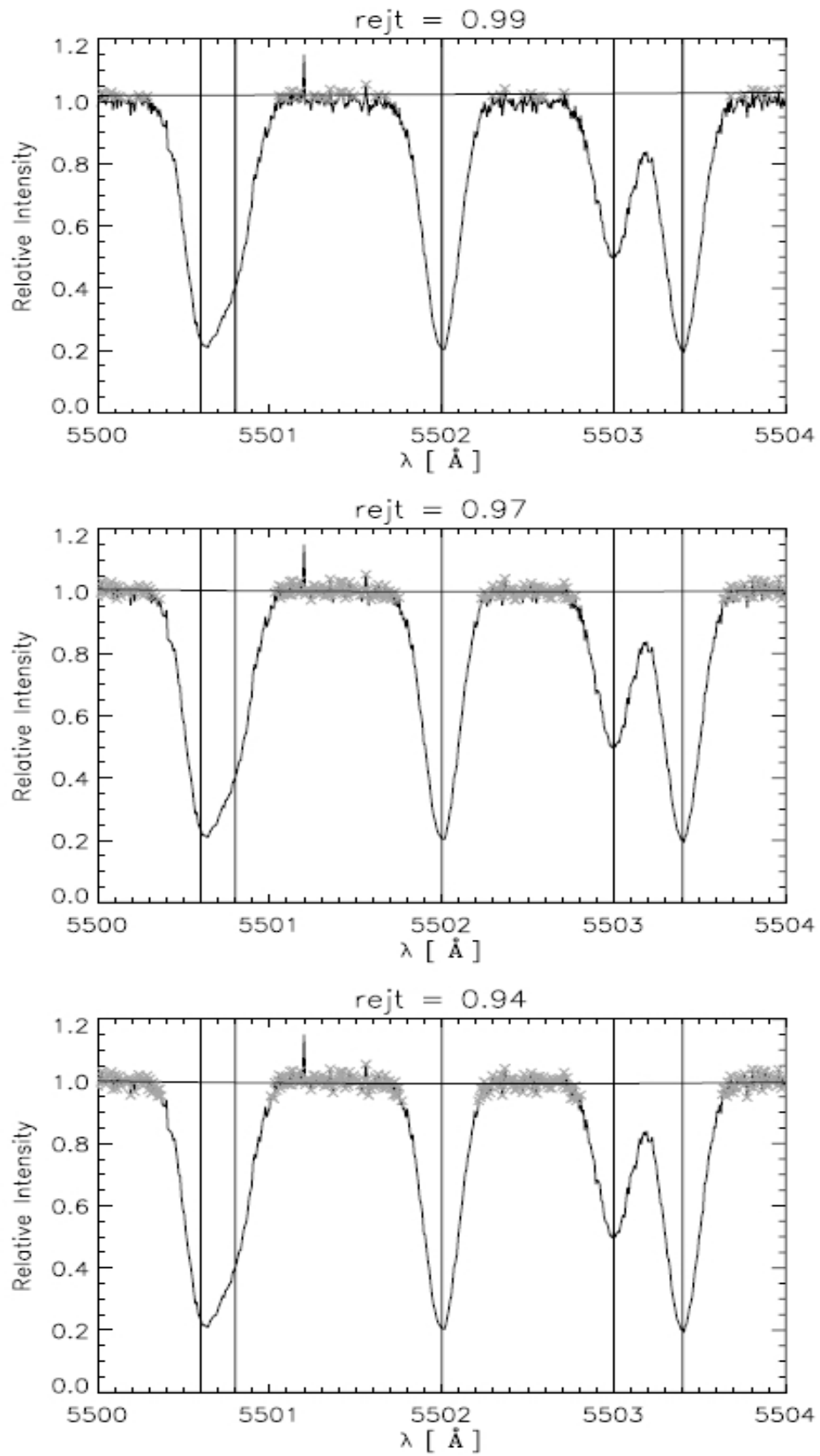


**Figure 2.2:** From Sousa et al. (2007). A synthetic spectrum region with a signal-to-noise ratio around 50. The filled line represents the fit to the local continuum through a 2nd-order polynomial based on the points that are marked as crosses in the spectrum. The variations induced by different values of the parameter  $rejt$  are readily visible.



between two consecutive lines (Sousa et al. 2007, Sousa 2013).

## 2.2 MOOG

MOOG is a code that is able to perform a variety of spectral line analysis and synthesis computations under LTE conditions. Typically, it is used to help with the determination of the chemical compositions of any given star. For the purposes of our work MOOG is used to measure the individual line abundances and to derive the parameters of the stellar atmosphere that fits the measured EWs (Sousa 2013, Sousa et al. 2008, Tsantaki et al. 2013).

Although one of the main features of MOOG is its ability to produce on-line graphics, this property is not required when using the ARES+MOOG method. The visualization of different plots can be useful in order to properly understand the dependency of the different parameters with individual abundances determination. But, since no higher plotting functions were required, a simple python code was used to visualize the required plots. The only purpose of this code was to show the parameter dependences and respective correlations (Sousa 2013).

MOOG needs to read the atomic data of each line to accomplish individual abundances calculations, therefore, an additional code was used in order to transform the output of ARES into a formatted file that could be read by MOOG (Sousa 2013).

Our iterative process starts by creating an atmospheric model using an initial guess value, running MOOG and plotting the results of the values determined by MOOG. An example of the correlation plots is shown in figure 2.3 (Sousa 2013). This figure clearly shows the correlations between the iron abundance,  $Ab(FeI)$ , and the excitation potential (E. P.), and the reduced equivalent width (R.W.). Also shown in the same plot are the respective slopes of the correlations, the difference between the average abundances of FeI and FeII ( $\langle Ab(FeI) \rangle - \langle Ab(FeII) \rangle$ ). Our iterative process will tweak the atmospheric parameters in such a way as to leave the slopes as close to zero as possible.

A minimization algorithm was used in order to compute the best parameters of the stars using MOOG. This minimization code has been described in Press et al. (1992), Saffe (2011).

Keep in mind that the errors of the parameter estimation are directly connected with the point dispersion present on each correlation. The dispersion is a result from several effects. Namely the quality of the spectra, the accuracy of the atomic data, and the errors of the EW determinations. In order to compute all the errors for each star a python algorithm was used.

We know from theoretical studies that there is a strong influence of the effective temperature value on the correlation  $\text{Ab}(\text{FeI})$  vs.  $E.P.$  There is also a strong dependency between microturbulence and the correlation  $\text{Ab}(\text{FeI})$  vs.  $R.W.$ , finally the value of the surface gravity influences the behaviour of  $\langle \text{Ab}(\text{FeI}) \rangle - \langle \text{Ab}(\text{FeII}) \rangle$  (Sousa 2013). The extent of the influence that each of these parameters has on the correlations will be described further in the following sections .

### 2.2.1 Dependence on the effective temperature

Considering that spectral lines are formed by electron transitions, the number of electrons in a given atomic level can, in a first approach, be approximated function with a dependency on  $T_{\text{eff}}$  . The different line strengths of the same element, each produced at a different energy level, will be a function dependent on the number of absorbers and  $T_{\text{eff}}$  . Any temperature estimated should, therefore, be such that the observed lines required the same element abundance, independently of the excitation potential.

Temperature changes influence dramatically the slopes of two of the correlations, as shown in figure 2.3. These changes manifest on the  $\text{Ab}(\text{FeI})$  vs.  $E.P.$  plot but also on the  $\text{Ab}(\text{FeI})$  vs.  $R.W.$ . Given that  $\text{Ab}(\text{FeI})$  vs.  $R.W.$  is a correlation more strongly influenced by microturbulence, the fact that both correlations are affected by a change in temperature, proves, once more, the interdependency of the various stellar parameters (Sousa 2013).

Since we know how variations on temperature affect the slope of  $\text{Ab}(\text{FeI})$  vs.  $E.P.$ , in practice it is possible to react accordingly and adjust the  $T_{\text{eff}}$  value. In fact, we know that when the temperature is underestimated the slope of the correlation is positive and when the temperature has been overestimated the slope is negative. Considering both of these behaviours it is a trivial matter to adjust our initial guesses simply by looking at the slope of the  $\text{Ab}(\text{FeI})$  vs.  $E.P.$  correlation (Sousa 2013).

### 2.2.2 Surface Gravity dependence

As stated above, the rate of ionization is mainly dependent on temperature but this is not the case of the recombination rate since, this rate depends, not only on the temperature but also on the electronic pressure of the stellar atmosphere. Given that electronic pressure is also inexorably linked to the stellar surface gravity these two parameters,  $T_{\text{eff}}$  and  $\log g$ , will manifest with opposing effects on the rate of recombination. Higher effective temperatures will increase the ionization rate but higher surface gravity

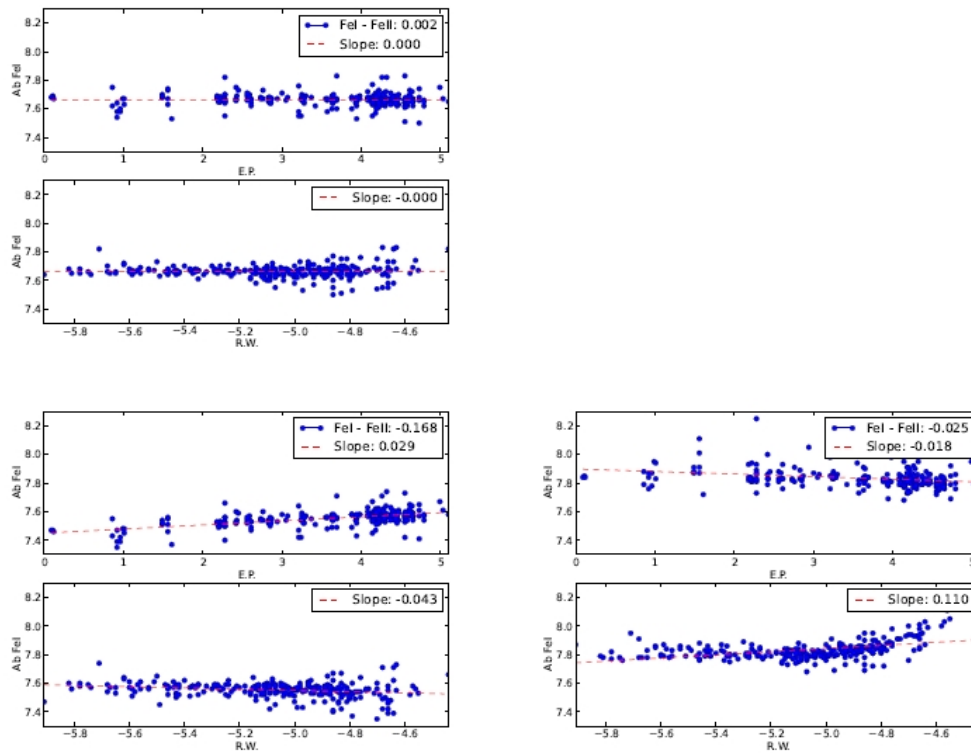


**Figure 2.3:** From Sousa (2013). Abundance of FeI as a function of excitation potential (E.P.) and reduced wavelength (R.W.). The top panel shows the result for the correct stellar parameters while in the bottom panels the temperature was changed to a lower value (5600K) - left panel, and an upper value (5900K) - right panel.

will increase the recombination rate (Gray 2005).

After having found a value for  $T_{\text{eff}}$ , it is necessary to fit the value of  $\log g$ . We know that the value of  $\log g$  has a strong effect on the correlation of  $\langle \text{Ab}(\text{FeI}) \rangle - \langle \text{Ab}(\text{FeII}) \rangle$ . Just as before, the behaviour of the slope of the correlation with respect to changes of the value of the surface gravity has been studied. When the value of the surface gravity has been underestimated the slope of the correlation is positive, in a symmetric behaviour, when the value of  $\log g$  has been overestimated the slope of the correlation becomes negative. We can use the ionization balance to constrain surface gravity since atomic iron is nearly unaffected by changes in surface gravity, while ionized iron changes with surface gravity, owing to the role that recombination assumes in those cases (Sousa 2013).

It is also an interesting fact that the changes in surface gravity have nearly no effect on the  $\text{Ab}(\text{FeI})$  vs. E.P. correlation. We can conclude from this lack of effect that the value of  $\log g$  obtained using this method is nearly independent of  $T_{\text{eff}}$  and vice-versa. This is a clear advantage of this method since the temperature and the iron abundance values are independently well-constrained. There is, however, a disadvantage inherent to this independence: the value of  $\log g$  is not well-constrained. Considering these determinations we can conclude that our values for temperature and iron abundance are well

determined but the value of  $\log g$  needs to be taken with a grain of salt as it relies on a very small number of ionized lines (Sousa 2013).

### 2.2.3 Microturbulence

Finally, the effect of microturbulence on spectral lines is more noticeable in strong spectral lines. Microturbulence is a non-thermal motion on the stellar atmosphere. It manifests itself by blue- or red-shifting the absorbers present in saturated lines and, consequently, it will affect the wings of the spectral lines and increase the amount of light absorbed by the line (Gray 2005).

The microturbulence parameter is closely connected with the saturation of the stronger iron lines. A good value for microturbulence will allow us to derive the same abundances for weak and strong lines. When the value of microturbulence is underestimated, the slope of the  $\text{Ab}(\text{FeI})$  vs. R.W. correlation will be positive but, when the value of microturbulence is overestimated, the correlation will have a negative slope (Sousa 2013).

### 2.2.4 Minimization code

The Downhill simplex method is a nonlinear optimization technique, and a well-known numerical method for problems with unknown derivatives. It can be used for the minimization of a function of  $n$  variables and it depends on the comparison of the variables at the vertices of a simplex. The simplex is constantly adapting itself and contracts to a local minimum (Saffe 2011, Press et al. 1992).

The method is computational compact. Its only assumption is that the function is continuous and has a unique minimum on the selected parameter area. Since the method can converge in local minima a restart criteria is applied as described in Press et al. (1992): if the solution has  $\chi^2 > 1$  the code will restart after reducing the tolerance criteria (Saffe 2011).



## Chapter 3.

### The TMCalc code

TMCalc is a software code that, using a given line-ratio calibration and metallicity calibration, is able to quickly and automatically determine the effective temperature and metallicities of a star having the values of the stellar spectra EWs. The temperature determined using TMCalc can easily be used to compare the spectroscopic temperature determined by other procedures.

The foundation of the use of line-ratios to obtain the temperature of a stellar atmosphere is the fact that spectral lines, as mentioned in chapter 1, change their strength with temperature and, as described in Gray (2005), the ratios of two spectral lines can be used as a thermometer for stars. The use of line-ratios can also minimize the errors of continuum determination.

The main factor behind the use of line-ratios to determine  $T_{\text{eff}}$  is a well performed calibration. In fact, TMCalc is only a tool but using the same line-ratio calibration any other software can be used to compute the same  $T_{\text{eff}}$  values. The most important aspect influencing the results of TMCalc is the calibration of the line-ratios used. The line-ratio calibrations are based mainly on weak FeI lines and other metals (e.g. Mg, Si, V, Ni, Ti, Cr) all of which depend mainly on temperature. The choice of iron can be easily justified by the simple fact that it has a high number of absorption lines. The element lines are also less dependent on other parameters such as surface gravity and microturbulence. As mentioned in chapter 1, changes in surface gravity will have a small impact on the strength of FeI lines, and any effect that microturbulence might have is almost non-existent since we are dealing with weak lines.

Because of this, a successful calibration requires only a pre-determination of the stellar parameters

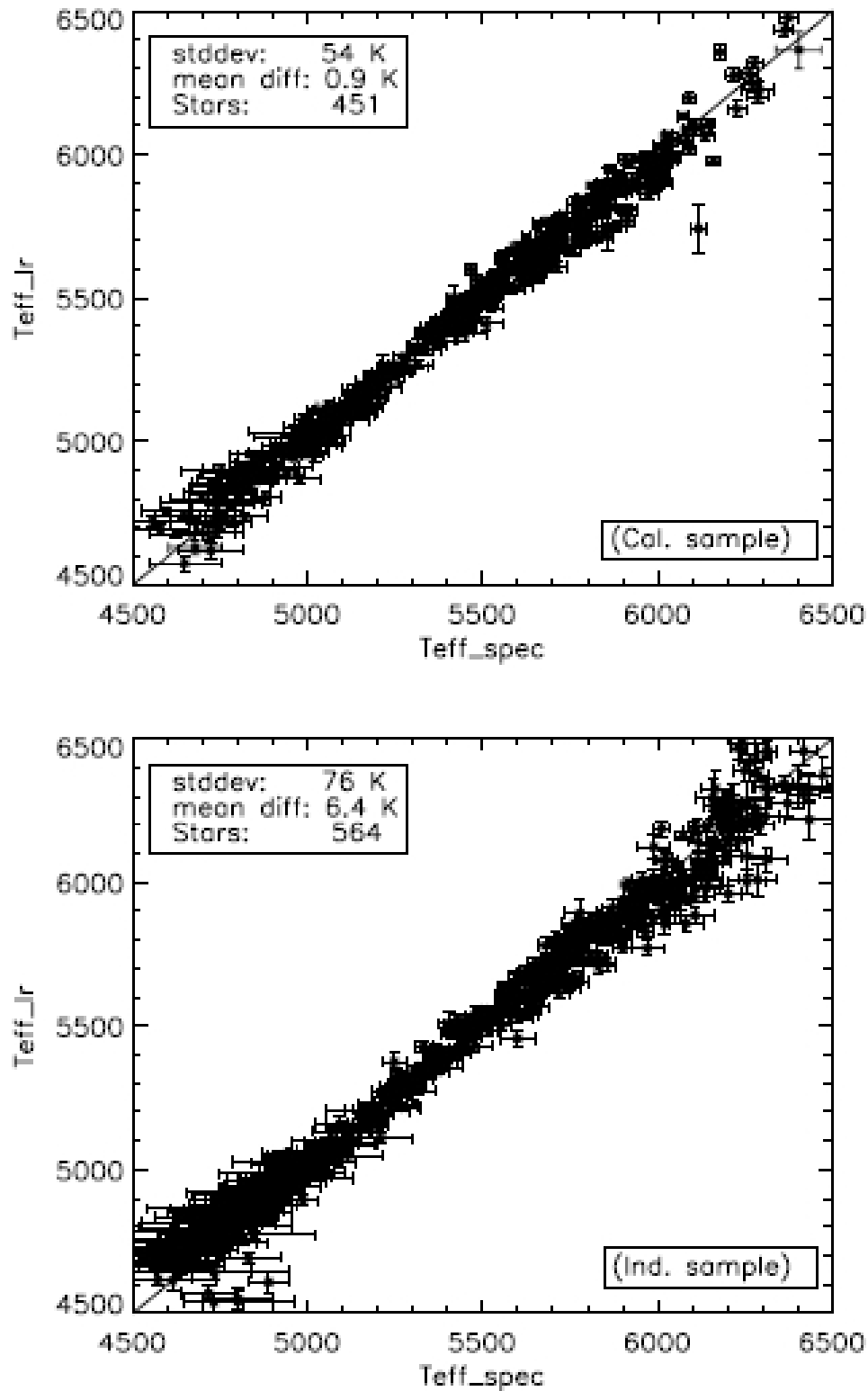
and respective errors of a calibration sample of stars.

Figure 3.1 shows the comparison of the temperatures obtained using this line-ratio calibration of Sousa et al. (2010) with those derived using the standard spectroscopic procedure Sousa et al. (2008). The top plot shows the comparison only for the sample of calibrator stars. As expected, the consistency is very good.

In the bottom plot of the same figure, the same comparison is shown for a sample of independent stars that were not used for the line-ratio calibration. Again, this plot shows a high degree of consistency. Both plots serve as reminders that the temperature inferred from the line-ratio is consistent with the standard spectroscopic method. This is a true indication that the line-ratio calibration can be used to determine the temperature of a star but the plot also shows the limits of stellar parameters for which the calibrations can be effectively used.

Since the line-ratio calibration is the most important factor for the TMCalc results, the development of a new calibration using more stars of different spectral types should produce a calibration file which can be used with TMCalc to estimate the temperatures of stars for a larger number of spectral types and larger sets of parameters.





**Figure 3.1:** From Sousa et al. (2012). In the top panel, the comparison between the effective temperatures derived from the ARES+MOOG method and the ones derived using TMCalc for the calibration sample of Sousa et al. (2010). In the bottom plot, a similar plot is shown but for the sample of stars of Sousa et al. (2010), a sample independent of the calibration. Both panels also show the mean difference and the standard deviation for the comparisons.

### 3.1 THE CALIBRATION ALGORITHM: GETCAL

The choice of which line-ratios to use is one of the most important factor which impacts the results of TMCalc. As such, it is of the utmost importance to properly determine the line-ratios by means of calibration techniques. Given this fact, one of the goals of this dissertation work was, given a sample of giant stars, to perform a recalibration of the line-ratios that TMCalc would use. To this effect, a recalibration code, the Great Tool for Calibrations, GeTCal, which performs the line-ratios recalibration was built using Python v2.66 and was structured in such a way as to be compatible with EW measurements from ARES and to take into account the parameters determined using the ARES+MOOG method, as well as the errors of those parameters. These errors were, in the context of our work, determined by a pre-existing python algorithm, however, GeTCal does not require the use of this additional python code, only that the errors of the parameters have been previously determined.

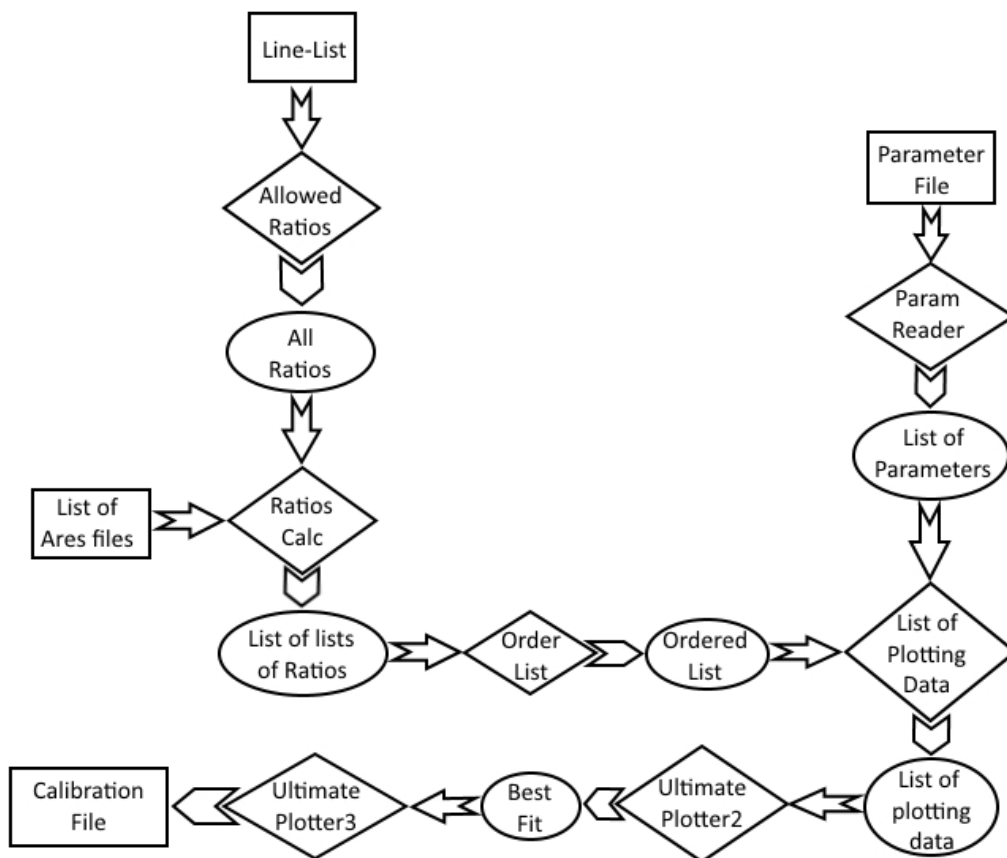


**Figure 3.2:** Flowchart of the calibration algorithm GeTCal. The boxes represent files, the losanges represent subroutines and the elipses represent data stored in memory.

The flowchart on figure 3.2 shows a simple overview of the algorithm that is the essence of GeT-

Cal. First GeTCal starts by reading the line list and computes which are the line-ratios, that fulfill the conditions already explained on the previous chapter:

1. The distance between the lines in the denominator and the numerator cannot be larger than 70 Å, thus diminishing the influence of continuum determination errors.
2. The excitation potential must be larger than 3 eV which will ensure that the lines of these elements vary greatly with temperature.

After having a list of the allowed line-ratios, the output files from ARES are read and all line-ratios are computed for each star. The list of ratios is then stored as a variable and reordered.

Concurrently the file which has the stellar parameters and respective errors is read and stored as a variable. Both variables are combined as a new variable.

A subsequent subroutine uses this variable. This is one of the most crucial steps of the entire algorithm, since this subroutine computes the best fit function for every line-ratio. Initially the value of the line-ratio and the temperature are extracted from the variable. An upper limit of 100 and a lower limit of 0.01 are chosen for the value of the ratios. These limits are chosen so that the difference between lines cannot be higher than two orders of magnitude, this way very strong lines which are not well fitted by Gaussian profiles are excluded, and weak lines, prone to measurement errors, are also removed. An additional cut is also put into place which does not allow line-ratio values higher than twice the mean of the values in order to remove outlier stars. Finally another cut is performed to the list of allowed ratios under the form of the well-known and robust Interquartile range(IQR) method, which is a measure of statistical dispersion that effectively trims the outliers (Upton et al. 1996). The IQR method requires the calculation of the IQR, which is defined as the difference between the third and first quartile of a data distribution,  $Q_3$  and  $Q_1$ , respectively. An outlier, using this method is any data point outside of the interval of values defined by  $[Q_1 - 1.5IQR, Q_3 + 1.5IQR]$ . This method is less sensitive to extreme outliers than other methods relying on sample variance or sample standard deviation (Upton et al. 1996).

After the outlier-removal procedure outlined above is performed, two functions are fitted to the remaining points, a linear and a 3rd degree polynomial function. Additional outliers are then removed by way of a  $2\text{-}\sigma$  cut which removes points that deviate from the fitted function more than twice the value

of the standard deviation ensuring a 95% confidence interval. As soon as this removal is done, the remaining datapoints are then used to once more fit a linear and 3rd degree polynomial function, and the coefficients of both fits are stored in a variable. An example of this  $2\text{-}\sigma$  cut is shown in figure 3.3, this plot shows the removal process for the ratio between lines SiI(6142.49 Å) and TiI (6126.22 Å). In the plot the black dots represent the stars removed by this final  $2\text{-}\sigma$  removal procedure. This particular ratio was chosen in order to show the good agreement of GeTCal when compared with the process used by Sousa et al. (2010) which presents a plot of the same line-ratio in figure 2 of that work.

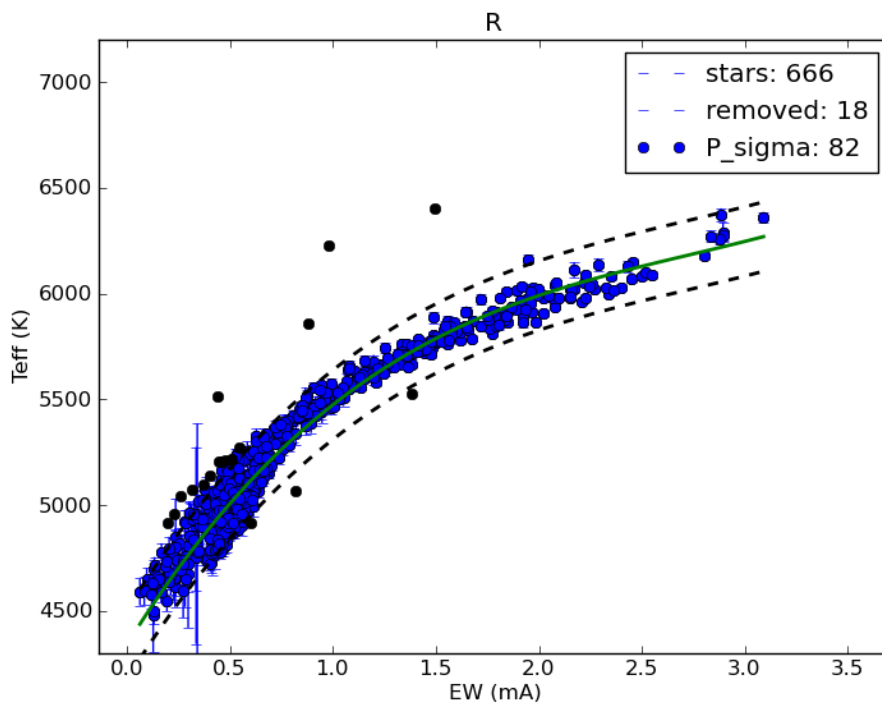


**Figure 3.3:** Plot of the 3rd degree polynomial fit for the ratio between the lines: SiI(6142.49 Å) and TiI (6126.22 Å). The dashed lines represent the 2-sigma of the fit. The black dots represent the stars removed using the  $2 - \sigma$  cut. Also shown is the error of the fit which is  $82K$ .

The outlier-removal and fitting processes described above are part of the UltimatePlotter2 subroutine and are repeated for the line-ratios,  $r$ , the inverse of the line-ratios,  $1/r$ , and also for the logarithm of the line-ratios,  $\log r$ . The subroutine plots these graphs, calculates the standard deviation of each fit, selects the function whose fit has the lowest standard deviation, and then stores the data of the chosen function as an output. Figure 3.4 shows the plots for the fits of the line-ratio between line 6739.52 Å, FeI, and line 6793.26 Å, FeI. The best fit function is then stored.

The best fit computed is stored on a TMCcalc compatible calibration file. As mentioned above the calibration file and the line-ratios chosen, ultimately depend on the type of stellar spectral type, the

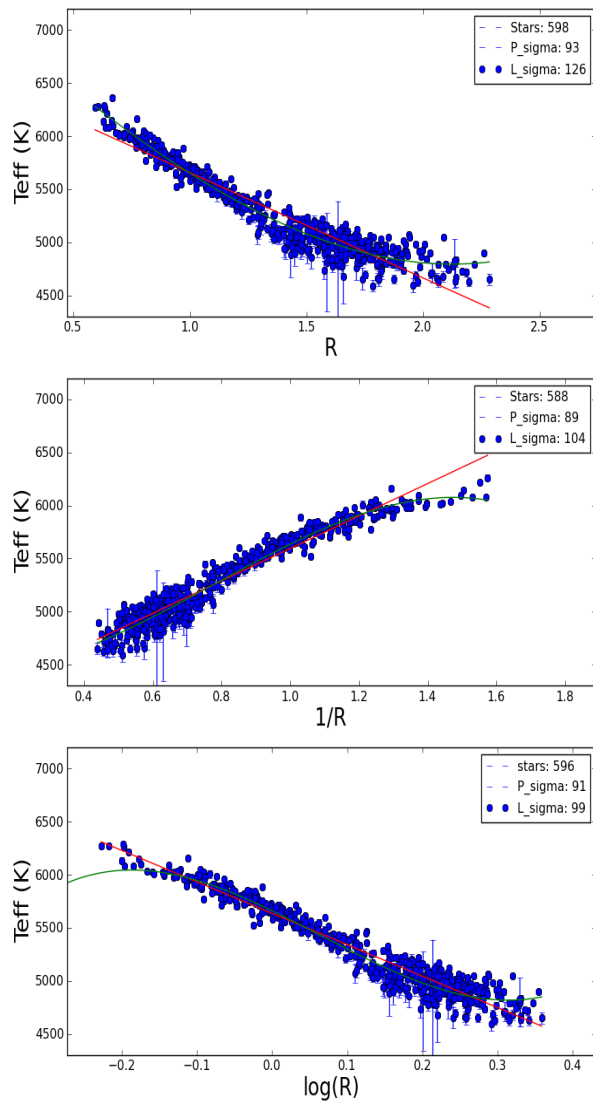


**Figure 3.4:** Plot of the fits for the ratio, the inverse of the ratio and the logarithm of the ratio between lines FeI 6739.52 Å and FeI 6793.26 Å, respectively from left to right. The blue lines are the linear fit, the green lines are the 3rd degree polynomial fit. The P\_sigma is the error of the 3rd degree polynomial fit, L\_sigma is the error of the linear fit and STARS is the number of stars used for the fit. In this case the polynomial of the inverse of the ratio was chosen as it had the lowest error,  $\sim 89K$ .

number of stars used in the calibration sample and, of course, on the quality of the calibration sample spectra itself.

## 3.2 THE NEW CALIBRATION

In order to obtain a new calibration file using GeTCal, a sample of stars to be used as the calibration sample had to be chosen. Therefore, in order to obtain the new calibration, two distinct datasets were used. One was the well-known and well-documented sample of 451 FGK-dwarf stars obtained by Sousa et al. (2008), hereafter Sousa-sample, the other was a sample of 256 K and G giant stars whose parameters had been determined by Alves et al. (2014), hereafter Alves-sample. The Alves-sample is composed of 256 GK giant stars, with spectra obtained using the UVES spectrograph at the La Silla Observatory. The spectra for all stars in the Alves-sample is high-resolution,  $\lambda/\Delta\lambda \sim 110000$ , and has a high S/N of  $\sim 150$ . The steps necessary to obtain the new calibration were: re-derivation of stellar parameters for the Sousa-sample and recalibration, attempt to use the new calibration in giants, final recalibration with a joint sample of the Sousa- and Alves-sample.

### Re-derivation and calibration of the Sousa sample

Even though the Sousa-sample has been well-documented, it has a problem, since the stars in this sample with temperatures below 5000 K have been shown to have higher offsets in the lower-temperature regime. It was, therefore, necessary to first re-determine the parameters for all the stars in the lower-temperature regime, in order to be more cautious in our analysis we defined stars in the lower-temperature regime those with  $T_{\text{eff}} < 5200$  K. In order to perform this re-determination a different line-list was required, specifically the Tsantaki line-list (Tsantaki et al. 2013). The Tsantaki line-list was obtained by carefully taking into account the effects that the lower temperatures have on solar-type stars, particularly in what weak spectral lines are concerned. The parameters for the Sousa-sample were redetermined using the Sousa line-list for the 310 stars with  $T_{\text{eff}} > 5200$  K and the Tsantaki line-list for the remaining 141 stars, using the described ARES+MOOG method. The reason for the redetermination of the parameters for the entire 451 stars of the Sousa-sample was simply to verify the homogeneity and consistency of our methods. The error determination code was applied to the results of the ARES+MOOG method and an output file with the parameters and errors was produced.

The redetermined stellar parameters of the 141 stars in the low-temperature regime were used to update the 451 FGK-dwarf star catalogue. A comparison with the work presented by Sousa et al.

(2008) showed only minor differences in the parameter values with the exception, as expected, of stars in the low-temperature regime since these parameters were computed using the Tsantaki line-list. Given that the ARES+MOOG method relies on a minimization method, it is no surprise that the values of the redetermined parameters are not equal to the values determined by Sousa et al. (2008). These small differences ( $\sim 10$  K) can be easily explained since they arise from numeric fluctuations of the minimization algorithm and the convergence criteria used.

GeTCal was used to obtain the new calibration files for TMCalc using the Sousa-sample for calibration, since the parameter values are similar for most Sousa-sample stars and the fact that GeTCal mostly emulates the calibration method presented in Sousa et al. (2010), the calibration file produced by GeTCal is quite similar to the calibration already made available with the current distribution of TMCalc. The calibration file produced from this sample uses 406 line-ratios. Hereafter this calibration will be referred to as the Sousa+Tsantaki, or S+T calibration. TMCalc computes the  $T_{\text{eff}}$  for each line-ratio and then computes the mean value weighted by the standard deviation of each line-ratio.

### Application of the S+T-calibration

As it is shown in figure 3.5, which uses the new S+T-calibration to obtain the temperature for the Sousa-sample, the significative difference is for stars in the low-temperature regime. An additional deviation from linearity was also observed for the stars with high temperatures. Both offsets have been addressed by the new calibration obtained with the GeTCal code. The comparison between the mean difference between the ARES+MOOG and the values obtained by the S+T calibration for the Sousa-sample can be seen in table 3.1. A refinement of the results obtained by the original calibration is observed, with the mean difference, previously  $-22$  K, becoming  $-1$  K and the standard deviation going from 69 K to 58 K.

We also had the values of the stellar parameters of the 256 giants of the Alves-sample, which had been kindly provided to us by Lisa Benamati. Nevertheless, we also performed a re-derivation of the parameters using the ARES+MOOG method as a way to again check the consistency of the results and ensure the homogeneity of our method. Again the difference in values was not significative ( $\sim 10$  K) and, as such, we choose to use the values provided by Lisa Benamati.

Given that we had a new improved S+T-calibration, we applied it with TMCalc to the Alves-sample

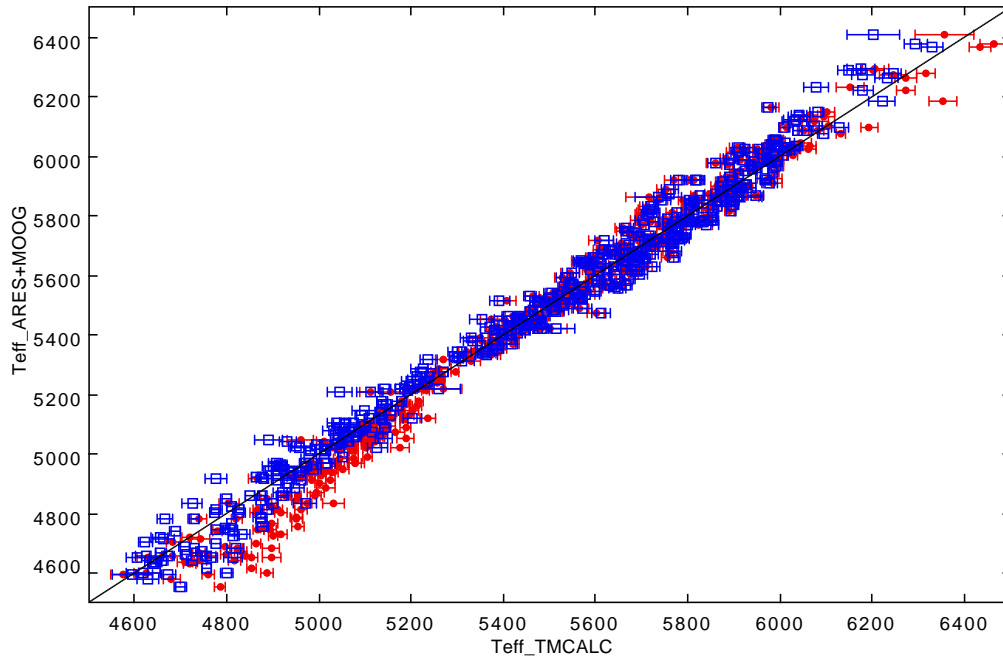


**Figure 3.5:** Comparison between the  $T_{\text{eff}}$  obtained using TMCALC and the  $T_{\text{eff}}$  obtained using the ARES+MOOG method for the sample of 451-FGK dwarf stars. The red circles are the results obtained for the original calibration, the blue open squares are the values using the new S+T calibration. The black line represents the identity line. A clear improvement can be seen for cool stars and for hot stars.

**Table 3.1:** Mean and standard deviation of the difference between the  $T_{\text{eff}}$  obtained using the ARES+MOOG method and the one obtained by applying each calibration file to TMCALC.

|             | Sousa-sample |              | Alves-sample |              |
|-------------|--------------|--------------|--------------|--------------|
| Calibration | Mean_dif (K) | $\sigma$ (K) | Mean_dif (K) | $\sigma$ (K) |
| Original    | -22          | 69           | -208         | 70           |
| S+T         | -1           | 58           | -168         | 62           |
| B           | 259          | 246          | 8            | 69           |
| J           | 17           | 77           | -32          | 58           |

of giant stars and checked how the results of the new temperatures obtained using S+T-calibration stacked up against the temperatures obtained using the standard ARES+MOOG method. Given that the differences were high, with a mean difference of  $-168$  K, see table 3.1, we computed with GeTCAL a calibration file for the Alves-sample. This new calibration file will, hereafter, be referred to as the B-calibration. Figure 3.6 shows the comparison between the results obtained using the S+T-calibration, in red circles, and the results of the B-calibration, open blue squares. It is clear that, for this sample, the B-calibration is a clear improvement.



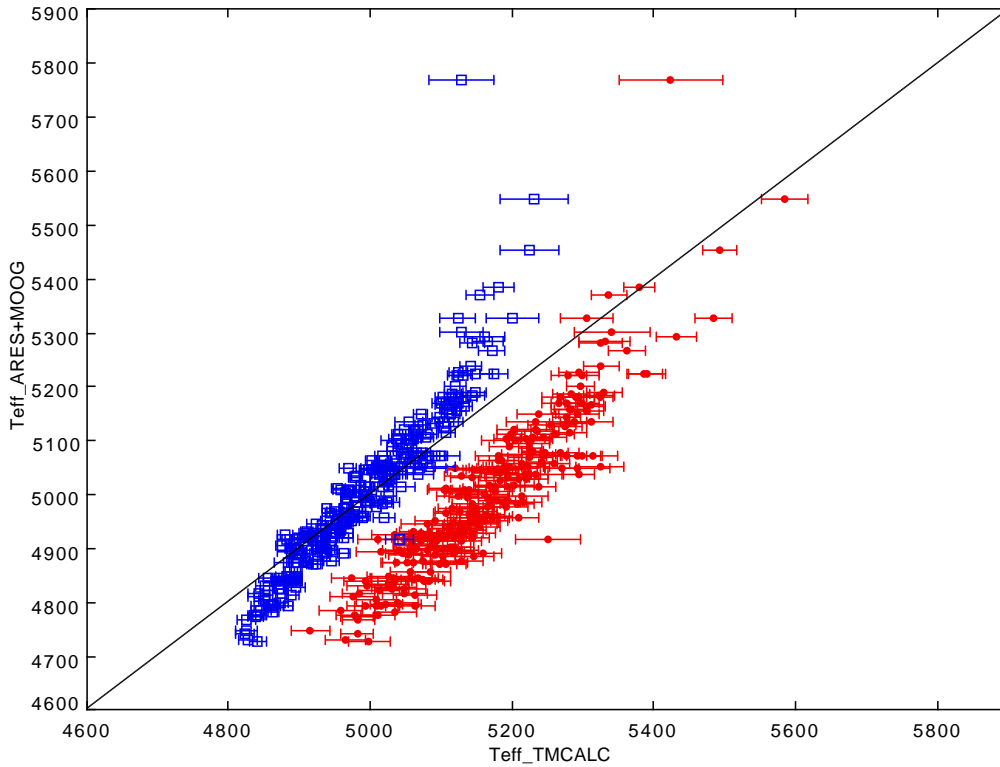


**Figure 3.6:** Comparison between the  $T_{\text{eff}}$  obtained using TMCALC and the  $T_{\text{eff}}$  obtained using the ARES+MOOG method for the sample of 256 giant stars. The red circles are the results obtained for the S+T-calibration, the blue open squares are the values using the new B calibration. The black line represents the identity line. A clear improvement can be observed.

### Obtaining the joint calibration

Since the B-calibration was obtained using the Alves-sample of giant stars, it was not expected that it would be useful for the determination of the temperatures of the Sousa-sample, composed by FGK-dwarfs. Nevertheless, the B-calibration was used in TMCALC to try to obtain the temperatures of the Sousa-sample. The result of this application of TMCALC and the comparison with the results obtained for the same sample using the S+T-calibration is shown in figure 3.7. Clearly the S+T-calibration is preferred for the Sousa-sample, as was expected. The B-calibration has a clear trend deviating from linearity. The mean difference between the ARES+MOOG and the TMCALC temperatures is of  $-1$  K using the S+T-calibration, but when using the B-calibration it reaches a value of  $259$  K as shown in table 3.1.

Given that neither the S+T- nor the B-calibrations were adequate for the full range of stars used, the calibration code was once again used. In this run of GeTCAL a joint sample, composed by both the Sousa- and the Alves-sample of stars was used. The reasoning for this joint calibration was the fact that using both FGK-dwarfs and giants as calibration the selected line-ratios would be such as

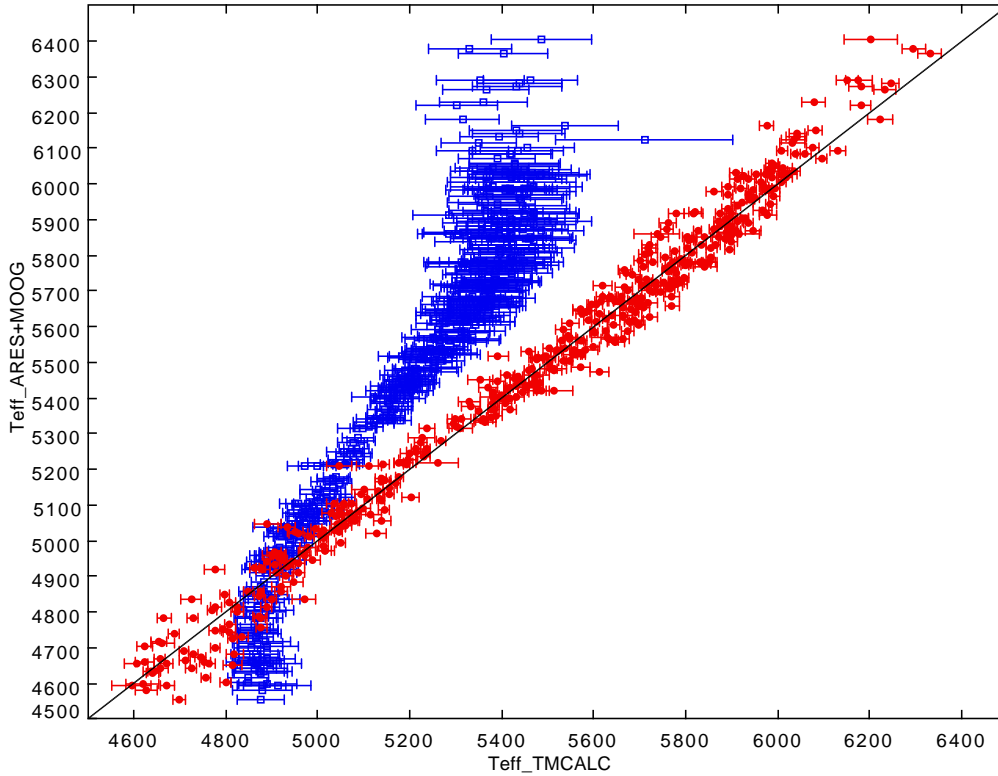


**Figure 3.7:** Comparison between the  $T_{\text{eff}}$  obtained using TMCALC and the  $T_{\text{eff}}$  obtained using the ARES+MOOG method for the sample of the 451 FGK-dwarfs. The red circles are the results obtained using the S+T-calibration, the blue open squares are the values using the B-calibration. The black line represents the identity line. A clear deviation from linearity is observed using the B-calibration.

to take into account the diversity of stellar evolutionary stages involved. The calibration file produced from this joint sample shall be referred during the remainder of this text as the J-calibration. Figure 3.8 shows the contrast between the temperature determination for the joint sample of stars using the S+T calibration and the J-calibration. Present in figure 3.8 is the clear improvement of the J-calibration over the S+T-calibration, a fact which can also be observed in table 3.1.

These results show that the J-calibration file can be accurately used by TMCALC to obtain temperatures for both FGK-dwarfs and giant stars. During the remainder of this work we used TMCALC in tandem with the J-calibration.

Table 3.2 presents a summary of the calibration files, showing the number of line-ratios present, the number of stars used for the calibration, the standard deviation obtained from comparing  $T_{\text{eff}}$  obtained by TMCALC for the calibration sample and the one from the ARES+MOOG method, the mean difference of the same comparison,  $T_{\text{eff}}$  of the coldest star in the sample and of the hottest and finally the lower and highest  $\log g$  in the calibration sample used.

The new calibration files will be made available as soon as GeTCAL is improved to also calibrate the

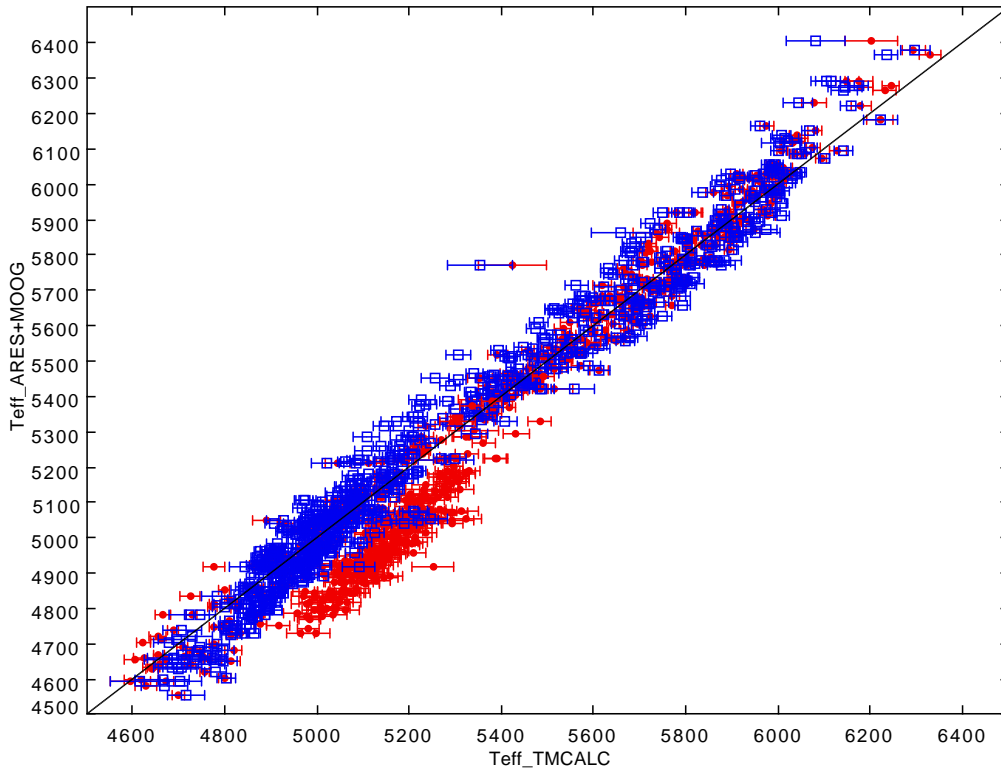


**Figure 3.8:** Comparison between the  $T_{\text{eff}}$  obtained using TMCALC and the  $T_{\text{eff}}$  obtained using the ARES+MOOG method for a sample composed by the 451 FGK-dwarfs and the Alves-sample of giants. The red circles are the results obtained using the S+T-calibration, the blue open squares are the values using the J-calibration. The black line represents the identity line. The J-calibration is able to compute the temperatures for both types of stars.

**Table 3.2:** Summary of each calibration file used.

| Calibration | num_ratios | num_stars | Mean_dif | $\sigma$ | $T_{\text{eff}} \text{ min}$ | $T_{\text{eff}} \text{ max}$ | $\log g \text{ min}$ | $\log g \text{ max}$ |
|-------------|------------|-----------|----------|----------|------------------------------|------------------------------|----------------------|----------------------|
| Original    | 433        | 451       | -22      | 69       | 4483                         | 6403                         | 3.63                 | 4.92                 |
| S+T         | 380        | 451       | -1       | 58       | 4483                         | 6403                         | 3.63                 | 4.92                 |
| B           | 752        | 257       | 8        | 69       | 4724                         | 5766                         | 2.37                 | 3.92                 |
| J           | 322        | 708       | -1       | 74       | 4483                         | 6403                         | 2.37                 | 4.92                 |

[Fe/H] and is presented in the Teixeira et al. (2014) paper, currently in preparation.



## Chapter 4.

### The new parameters

The ARES+MOOG method detailed above and the results of TMCalc using the J-calibration file were used in tandem in order to re-derive stellar parameters for our spectra. The following chapter describes the new derived parameters. The comparison between the old parameters and the newly determined ones is also shown in the cases when it is applicable. The ASCII tables of the new parameters have been made available online on [http://astro.up.pt/~gteixeira/new\\_parameters/](http://astro.up.pt/~gteixeira/new_parameters/).

#### 4.1 NEW PARAMETER TABLES

The first table, a sample of which is shown in table 4.1, shows the rederivation of parameters for the Sousa-sample. Significant differences were only found for stars in the low-temperature regime,  $T_{\text{eff}} < 5200$  K, which were computed using the Tsantaki line-list. The number of stars rederived using the Tsantaki line-list was 141 FGK-dwarfs from the full Sousa-sample. The full table can be found in [http://astro.up.pt/~gteixeira/new\\_parameters/sousa\\_jcal\\_table.dat](http://astro.up.pt/~gteixeira/new_parameters/sousa_jcal_table.dat). As was previously shown there is a good agreement between the  $T_{\text{eff}}$  obtained using the J-calibration in TMCalc and the temperature obtained using the ARES+MOOG method. The temperature value and the respective errors obtained using TMCalc are also present in the table under the names `Teff_tm` and `err_Teff_tm` respectively. The standard deviation of the difference between the ARES+MOOG method and the TMCalc computation with the J-calibration was 77 K.

A similar table was produced for the Alves-sample, a sample of this is shown in table 4.2. For this

## Spectroscopic Calibrations for a Better Characterization of Stars and Planets

**Table 4.1:** Parameters for the Sousa-sample of FGK-dwarf stars. This is only a small sample of the parameters. The full table can be found at [http://astro.up.pt/~gteixeira/new\\_parameters/sousa\\_jcal\\_table.dat](http://astro.up.pt/~gteixeira/new_parameters/sousa_jcal_table.dat).

| Star     | $T_{\text{eff}}$ | $er_{T_{\text{eff}}}$ | $\log g$ | $er_{\log g}$ | $vt$ | $er_{vt}$ | M/H   | $er_{M/H}$ | $T_{\text{eff\_tm}}$ | $er_{T_{\text{eff\_tm}}}$ | $T_{\text{eff\_diff}}$ |
|----------|------------------|-----------------------|----------|---------------|------|-----------|-------|------------|----------------------|---------------------------|------------------------|
| HD10002  | 5313             | 44                    | 4.4      | 0.07          | 0.82 | 0.09      | 0.17  | 0.03       | 5145                 | 22                        | 168                    |
| HD100508 | 5449             | 61                    | 4.42     | 0.09          | 0.86 | 0.09      | 0.39  | 0.05       | 5257                 | 29                        | 192                    |
| HD100777 | 5536             | 26                    | 4.33     | 0.05          | 0.81 | 0.04      | 0.25  | 0.02       | 5447                 | 17                        | 89                     |
| HD10166  | 5221             | 31                    | 4.48     | 0.07          | 0.74 | 0.07      | -0.39 | 0.02       | 5159                 | 33                        | 62                     |
| HD10180  | 5911             | 19                    | 4.39     | 0.03          | 1.11 | 0.02      | 0.08  | 0.01       | 5874                 | 14                        | 37                     |
| HD102117 | 5657             | 24                    | 4.31     | 0.04          | 0.99 | 0.03      | 0.28  | 0.02       | 5556                 | 19                        | 101                    |
| HD102365 | 5629             | 29                    | 4.44     | 0.03          | 0.91 | 0.04      | -0.29 | 0.02       | 5659                 | 25                        | -30                    |
| HD102438 | 5560             | 13                    | 4.41     | 0.03          | 0.84 | 0.02      | -0.29 | 0.01       | 5649                 | 18                        | -89                    |
| HD104263 | 5477             | 23                    | 4.34     | 0.04          | 0.81 | 0.03      | 0.02  | 0.02       | 5422                 | 10                        | 55                     |
| HD104982 | 5692             | 14                    | 4.44     | 0.02          | 0.91 | 0.02      | -0.19 | 0.01       | 5756                 | 12                        | -64                    |
| ...      | ...              | ...                   | ...      | ...           | ...  | ...       | ...   | ...        | ...                  | ...                       | ...                    |

**Table 4.2:** Parameters for the Alves-sample of giant stars. This is only a small sample of the parameters. The full table can be found at [http://astro.up.pt/~gteixeira/new\\_parameters/benamati\\_jcal\\_table.dat](http://astro.up.pt/~gteixeira/new_parameters/benamati_jcal_table.dat).

| Star     | $T_{\text{eff}}$ | $er_{T_{\text{eff}}}$ | $\log g$ | $er_{\log g}$ | $vt$ | $er_{vt}$ | M/H   | $er_{M/H}$ | $T_{\text{eff\_tm}}$ | $er_{T_{\text{eff\_tm}}}$ | $T_{\text{eff\_diff}}$ |
|----------|------------------|-----------------------|----------|---------------|------|-----------|-------|------------|----------------------|---------------------------|------------------------|
| HD74006  | 5766             | 149                   | 3.92     | 0.151         | 4.28 | 0.422     | -0.02 | 0.116      | 5355                 | 71                        | 411                    |
| HD177389 | 5102             | 24                    | 3.5      | 0.04          | 1.08 | 0.032     | -0.03 | 0.02       | 5075                 | 7                         | 27                     |
| HD6793   | 5367             | 33                    | 3.49     | 0.105         | 1.7  | 0.041     | 0.03  | 0.027      | 5225                 | 17                        | 142                    |
| HD175145 | 5382             | 23                    | 3.49     | 0.057         | 1.41 | 0.028     | 0.02  | 0.021      | 5283                 | 15                        | 99                     |
| HD6080   | 5118             | 25                    | 3.46     | 0.038         | 1.12 | 0.031     | -0.07 | 0.02       | 5081                 | 10                        | 37                     |
| HD87896  | 5324             | 37                    | 3.46     | 0.094         | 1.51 | 0.042     | 0.13  | 0.03       | 5171                 | 31                        | 153                    |
| HD67762  | 5010             | 27                    | 3.42     | 0.055         | 1.1  | 0.032     | -0.01 | 0.02       | 4973                 | 8                         | 37                     |
| HD141832 | 5046             | 43                    | 3.41     | 0.069         | 1.3  | 0.054     | 0.11  | 0.035      | 4984                 | 14                        | 62                     |
| HD140329 | 5043             | 30                    | 3.4      | 0.066         | 1.15 | 0.036     | 0.02  | 0.022      | 5018                 | 9                         | 25                     |
| HD85612  | 5108             | 22                    | 3.38     | 0.039         | 1.18 | 0.026     | -0.05 | 0.018      | 5075                 | 8                         | 33                     |
| ...      | ...              | ...                   | ...      | ...           | ...  | ...       | ...   | ...        | ...                  | ...                       | ...                    |

case the standard deviation of the difference between the temperatures obtained by each method was of 58 K.

## 4.2 AN INDEPENDENT 56 GIANT-STAR SAMPLE

The parameter derivation for an independent sample of 56 giant stars (Santos et al. 2009) was performed using the ARES+MOOG method and, subsequently, TMCALC. Table 4.3 shows a sample of the determined parameters. The full table can be found in [http://astro.up.pt/~gteixeira/new\\_parameters/56\\_independent\\_jcal\\_table.dat](http://astro.up.pt/~gteixeira/new_parameters/56_independent_jcal_table.dat). Looking at figure 4.1, showing a plot of the TMCALC temperatures using the J-calibration against a plot of the ARES+MOOG temperatures, it is clear that there are some outliers which can be explained if we look at the fact that these stars have low temperatures and extremely low  $\log g$  values, thus making the EW measurement harder.

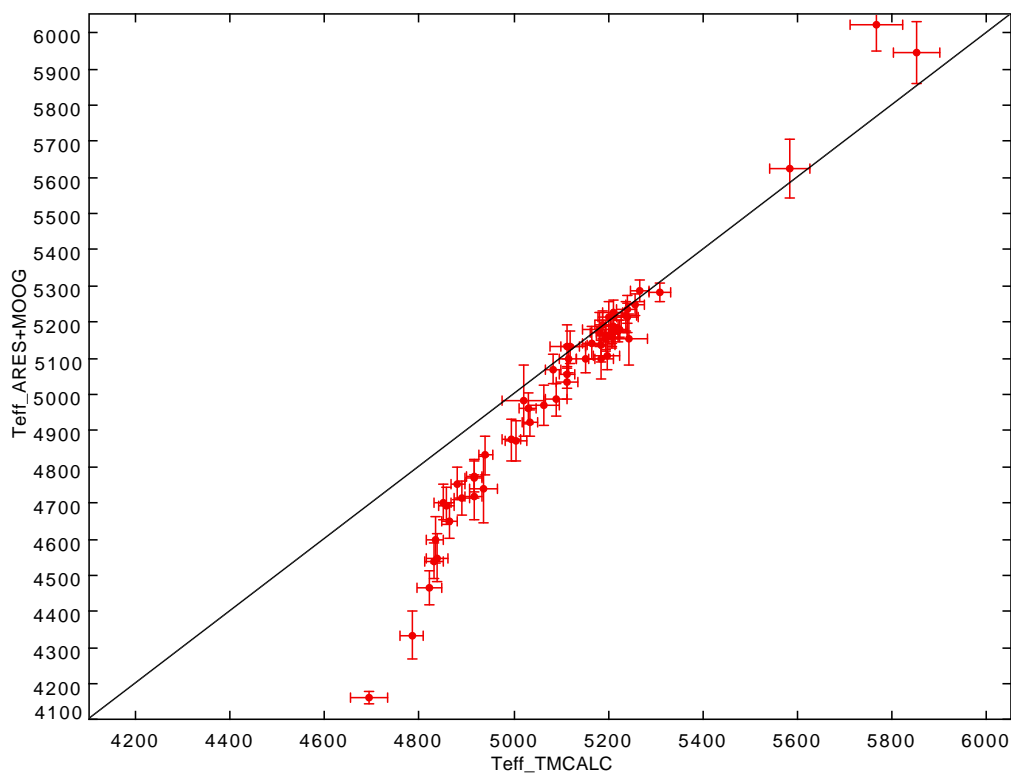


**Figure 4.1:** Comparison between the  $T_{\text{eff}}$  obtained using TMCALC and the  $T_{\text{eff}}$  obtained using the ARES+MOOG method for the sample of 56 giant stars used. The black line represents the identity line.

**Table 4.3:** Parameters for the sample of 56 giant stars. This is only a small sample of the parameters. The full table can be found at [http://astro.up.pt/~gteixeira/new\\_parameters/56\\_independent\\_j\\_cal\\_table.dat](http://astro.up.pt/~gteixeira/new_parameters/56_independent_j_cal_table.dat).

| Star          | $T_{\text{eff}}$ | err_ $T_{\text{eff}}$ | $\log g$ | err_ $\log g$ | vt   | err_vt | M/H  | err_M/H | T_tm | err_T_tm | T_diff |
|---------------|------------------|-----------------------|----------|---------------|------|--------|------|---------|------|----------|--------|
| IC2714No110   | 5127.0           | 45                    | 2.84     | 0.11          | 1.52 | 0.05   | 0.04 | 0.04    | 5119 | 19       | 8      |
| IC2714No53    | 5165.0           | 37                    | 2.77     | 0.13          | 1.5  | 0.04   | 0.03 | 0.03    | 5181 | 21       | -16    |
| IC2714No87    | 5210.0           | 42                    | 2.81     | 0.13          | 1.57 | 0.05   | 0.04 | 0.04    | 5202 | 24       | 8      |
| IC4651No10393 | 4827.0           | 53                    | 2.48     | 0.24          | 1.26 | 0.06   | 0.06 | 0.04    | 4941 | 16       | -114   |
| IC4651No7646  | 4957.0           | 41                    | 2.75     | 0.13          | 1.5  | 0.04   | 0.1  | 0.04    | 5030 | 18       | -73    |
| IC4651No9122  | 4686.0           | 51                    | 2.6      | 0.20          | 1.38 | 0.06   | 0.09 | 0.04    | 4858 | 16       | -172   |
| IC4756No125   | 5172.0           | 29                    | 2.93     | 0.09          | 1.45 | 0.03   | 0.01 | 0.03    | 5222 | 19       | -50    |
| IC4756No38    | 5177.0           | 24                    | 3.01     | 0.07          | 1.34 | 0.03   | 0.03 | 0.02    | 5223 | 17       | -46    |
| IC4756No42    | 5245.0           | 30                    | 3.1      | 0.07          | 1.37 | 0.03   | 0.03 | 0.03    | 5258 | 20       | -13    |
| NGC2287No21   | 4157.0           | 18                    | 1.15     | 0.18          | 2.26 | 0.02   | 0.32 | 0.19    | 4695 | 39       | -538   |
| ...           | ...              | ...                   | ...      | ...           | ...  | ...    | ...  | ...     | ...  | ...      | ...    |

### 4.3 THE GAIA-ESO SURVEY BENCHMARK STAR SAMPLE

The GAIA-ESO Public Spectroscopic Survey aims to obtain quality spectroscopy for nearly 100000 stars, down to magnitude 19 and will cover systematically the major components of our galaxy. The survey is expected to deliver improved astrophysical parameters for each star using, as basis, CoRoT benchmark stars. These stars have their  $\log g$  values well-determined from asteroseismology. As such we used TMCalc to obtain the temperatures of these stars with the J-calibration file.

The computation of the temperature values for CoRoT benchmark stars was performed using our J-calibration. These new temperature values will be used in the remainder of the GAIA-ESO survey program. A plot similar to the ones presented before, comparing the results obtained by TMCalc and the ARES+MOOG method is shown as figure 4.2. The cooler stars deviate further from the identity line, which is not a surprise considering that the catalogue of benchmark stars has some members that are well into the low-temperature regime with temperatures below our calibration samples. As such it was decided that the survey would only consider the rederivation of stars within the temperature interval  $4900 \text{ K} < T_{\text{eff}} < 6500 \text{ K}$ . This consideration allows for a minimization of errors. A sample of this table is presented in table 4.4.



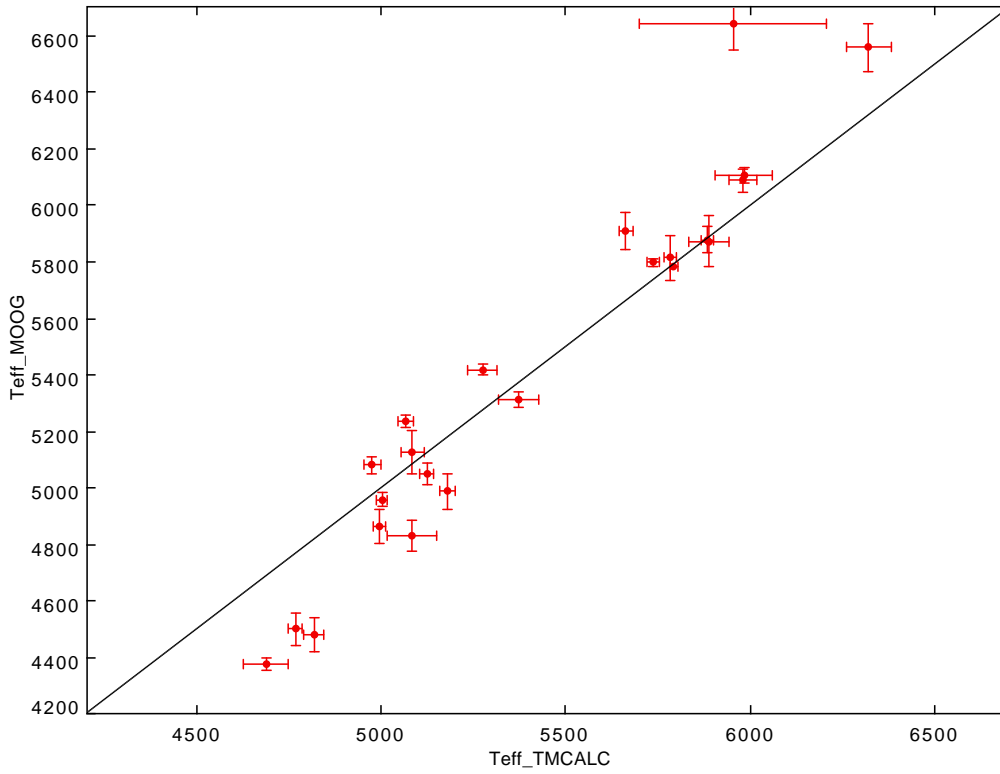


**Figure 4.2:** Comparison between the  $T_{\text{eff}}$  obtained using TMCALC and the  $T_{\text{eff}}$  obtained using the ARES+MOOG method for the COROT benchmark stars. The black line represents the identity line.

**Table 4.4:** Parameters for the sample of COROT benchmark stars. This is only a small sample of the parameters. The full table can be found at [http://astro.up.pt/~gteixeira/new\\_parameters/benchmark\\_jcal\\_table.dat](http://astro.up.pt/~gteixeira/new_parameters/benchmark_jcal_table.dat).

| Star      | $T_{\text{eff}}$ | $er_{T_{\text{eff}}}$ | $\log g$ | $er_{\log g}$ | Fe/H  | $er_{\text{Fe/H}}$ | V    | $er_V$ | $T_{\text{eff\_tm}}$ | $er_{T_{\text{eff\_tm}}}$ | $T_{\text{eff\_diff}}$ |
|-----------|------------------|-----------------------|----------|---------------|-------|--------------------|------|--------|----------------------|---------------------------|------------------------|
| 18Sco     | 5810             | 80                    | 4.44     | 0.03          | 0.03  | 0.03               | 1.07 | 0.2    | 5784                 | 17                        | 26                     |
| 61CygA    | 4374             | 22                    | 4.63     | 0.04          | -0.33 | 0.38               | 1.07 | 0.04   | 4687                 | 62                        | -313                   |
| alfCenA   | 5792             | 16                    | 4.3      | 0.01          | 0.26  | 0.08               | 1.2  | 0.07   | 5738                 | 17                        | 54                     |
| alfCenB-w | 5231             | 20                    | 4.53     | 0.03          | 0.22  | 0.1                | 0.99 | 0.31   | 5065                 | 21                        | 166                    |
| Arcturus  | 4286             | 35                    | 1.64     | 0.06          | -0.52 | 0.08               | 1.58 | 0.12   | 4711                 | 27                        | -425                   |
| betGem    | 4858             | 60                    | 2.9      | 0.06          | 0.13  | 0.16               | 1.28 | 0.21   | 4994                 | 17                        | -136                   |
| betHyi-w  | 5873             | 45                    | 3.98     | 0.02          | -0.04 | 0.06               | 1.26 | 0.05   | 5884                 | 16                        | -11                    |
| betVir    | 6083             | 41                    | 4.1      | 0.02          | 0.24  | 0.07               | 1.33 | 0.09   | 5981                 | 37                        | 102                    |
| delEri-w  | 4954             | 26                    | 3.75     | 0.02          | 0.06  | 0.05               | 1.1  | 0.22   | 5001                 | 13                        | -47                    |
| epsEri-w  | 5076             | 30                    | 4.6      | 0.03          | -0.09 | 0.06               | 1.14 | 0.05   | 4976                 | 22                        | 100                    |
| ...       | ...              | ...                   | ...      | ...           | ...   | ...                | ...  | ...    | ...                  | ...                       | ...                    |

## 4.4 LIMITS OF THE NEW CALIBRATION

Figure 4.3, plots the TMCALC  $T_{\text{eff}}$  against the values of ARES+MOOG for all samples determined by our J-calibration. The colour code in this plot shows the value of  $\log g$ , hotter colors for higher  $\log g$ . It is apparent that outlier stars have low values of temperature while also having low  $\log g$ . This translates into spectra which will have an abundance of blending effects and, therefore, makes the measurements of EWs more problematic. Based on this we have empirically set limits to the applicability of the J-calibration. These limits are shown in table 4.5.

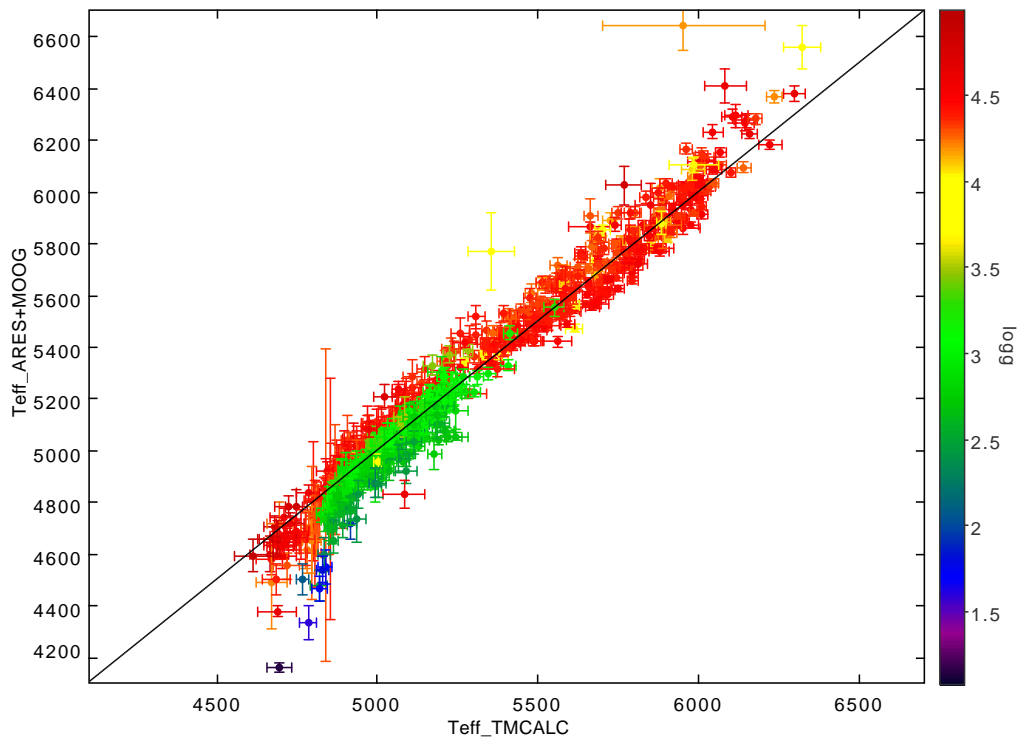


**Figure 4.3:** Comparison between the  $T_{\text{eff}}$  obtained using TMCALC and the  $T_{\text{eff}}$  obtained using the ARES+MOOG method for all stars used during our study. The black line represents the identity line. The colour code shows the value of  $\log g$  of each star. It is clear that most outliers are stars with very low  $\log g$  values.

**Table 4.5:** Limits of applicability of the J-calibration.

| $T_{\text{eff}}$ | $\log g$ | [Fe/H]      |
|------------------|----------|-------------|
| [4500, 6500]     | [2, 4.9] | [-0.8, 0.5] |

## Chapter 5.

### Summary

A computer code, GeTCal, was built which is capable of, given a sample of stars with their EWs, and their stellar parameters, create a calibration file based on line-ratios. This file is compatible with the TMCalc code and can be used in tandem in order to quickly obtain stellar temperatures for stars of the same spectral type as the ones used to produce the calibration file.

New stellar parameters for the 451 FGK-dwarf sample of Sousa et al. (2008) were obtained using the Tsantaki line-list (Tsantaki et al. 2013) for the 141 stars with  $T_{\text{eff}} < 5200$  K.

We have used the new parameters of the 451 FGK-dwarfs to obtain a calibration file and tested it using TMCalc on a sample of 256 giant stars provided by Lisa Benamati. Since the temperatures obtained for the Alves-sample using this calibration had a mean difference of  $-168$  K from the values obtained with ARES+MOOG it was apparent that this calibration was not adequate for giant stars.

A second calibration file was obtained using the Alves-sample as calibration sample. Although this calibration reduced the mean difference between the ARES+MOOG and the TMCalc values for the Alves-sample to 8 K it couldn't be used for the Sousa-sample. The mean difference between the ARES+MOOG values and the TMCalc for the Sousa-sample using the B-calibration was 259 K.

A third calibration file, J-calibration, was obtained using for calibration a joint sample composed of the Sousa- and Alves-samples. This mixed calibration file when applied to TMCalc returns a mean difference of 17 K and  $-32$  K for the Sousa- and Alves-samples respectively.

Using the J-calibration on TMCalc we were able to obtain new temperature values for an independent sample of 56-giant stars and for the COROT benchmark stars. The analysis of these new values

allowed us to empirically limit the applicability of the J-calibration to the following limits:

$$4500 \text{ K} < T_{\text{eff}} < 6500 \text{ K}, 2 < \log g < 4.9, -0.8 < [Fe/H] < 0.5.$$

The new CoRoT benchmark temperature values will be used as the *de facto* values for the GAIA-ESO survey CoRoT collaboration. They will become increasingly important as the GAIA-ESO survey progresses. One of the data products of the survey is improved astrophysical parameters so the importance of well-determined parameters for the benchmark stars cannot be overstated.

The J-calibration has been successfully tested for FGK-dwarfs and giants within the previously mentioned limits. The  $T_{\text{eff}}$  determined using TMCalc is also dependent on the quality of the S/N of the spectra and the wavelength windows used.

All parameter tables have been provided in [http://astro.up.pt/~gteixeira/new\\_parameters/](http://astro.up.pt/~gteixeira/new_parameters/). The calibration file itself will be released later.

The new calibration will also be part of one of the recipes in the ESPRESSO data analysis pipelines.

A limitation of the GeTCal code is that it does not, as of yet, produce another calibration file for TMCalc that allows for an accurate determination of the metallicity values for the stars.

## 5.1 FUTURE WORK

Although GeTCal has been coded to produce a calibration file which will be used by TMCalc to successfully determine the  $T_{\text{eff}}$  value there is still an additional calibration that we wish to include in the GeTCal code. As of now GeTCal does not calibrate TMCalc in order to obtain [Fe/H] values. Our immediate goal is to add the metallicity calibration and be able to produce one additional calibration file which will take metallicity into account. The new addition to the GeTCal will emulate the calibration method described in Sousa et al. (2012).

After this additional calibration has been added to the GeTCal code we hope to distribute the GeTCal to the community packaged with TMCalc. As soon as this final addition is ready we will present the GeTCal code in an upcoming paper currently in preparation (Teixeira et al. 2014). We will once again perform a calibration using this new version of GeTCal and will reobtain the parameters for all stars of the sample.

One additional work that could be interesting to do is to use a larger sample of spectra for a greater

number of spectral types at different evolutionary stages and produce calibration files. This calibration, having a broad interval of parameters, could be used to accurately compute the temperature and metallicity of stars with spectral types in a wide range. As an ultimate goal a larger calibration sample would be able to produce a stable and encompassing calibration file for TMCalc.



# Bibliography

Adibekyan, V. Z., González Hernández, J. I., Delgado Mena, E., Sousa, S. G., Santos, N. C., Israelian, G., Figueira, P., Bertran de Lis, S. 2014, *A&A*, 564, L15 <http://dx.doi.org/10.1051/0004-6361/201423435>

Alves, S. et al., 2014, *in preparation*

Carroll, B. W., & Ostlie, D. A. 2006, *An introduction to modern astrophysics and cosmology*

Casagrande, L., Ramírez, I., Meléndez, J., Bessell, M., Asplund, M. 2010, *A&A*, 512, A54 <http://dx.doi.org/10.1051/0004-6361/200913204>

Desidera, S., Covino, E., Messina, S., D'Orazi, V., Alcalá, J. M., Brugaletta, E., Carson, J., Lanzafame, A. C., Launhardt, R. 2011, *A&A*, 529, A54 <http://dx.doi.org/10.1051/0004-6361/201016267>

Gray, D. F. 1994, *PASP*, 106 <http://adsabs.harvard.edu/abs/1994PASP...106.1248G>

Gray, D. F. 2004, *Advances in Space Research*, 34, 308 <http://dx.doi.org/10.1016/j.asr.2003.01.023>

Gray, D. F. 2005, *The Observation and Analysis of Stellar Photospheres*, 3rd Edition, ISBN 0521851866. , UK: Cambridge University Press, 2005

González Hernández, J. I., Bonifacio, P. 2009, *A&A*, 497 <http://dx.doi.org/10.1051/0004-6361/200810904>

Kovtyukh, V. V., Soubiran, C., Belik, S. I., Gorlova, N. I. 2003, *A&A*, 411 <http://dx.doi.org/10.1051/0004-6361:20031378>

- Mortier, A., Santos, N. C., Sousa, S. G., Adibekyan, V. Z., Delgado Mena, E., Tsantaki, M., Israelian, G., Mayor, M. 2013, *A&A*, 557, A70 <http://dx.doi.org/10.1051/0004-6361/201321641>
- Press, W. H., Teukolsky, S. A., Vetterling, W. T., Flannery, B. P. 1992, *Numerical Recipes: The Art of Scientific Computing*, 2nd edition. Cambridge University Press, Cambridge
- Saffe, C. 2011, *Revista Mexicana de Astronomía y Astrofísica*, 47
- Santos, N. C., Israelian, G., Mayor, M. 2004, *A&A*, 415 <http://dx.doi.org/10.1051/0004-6361:20034469>
- Santos, N. C., Lovis, C., Pace, G., Melendez, J., Naef, D. 2009, *A&A*, 493 <http://dx.doi.org/10.1051/0004-6361:200811093>
- Sousa, S. G., Santos, N. C., Israelian, G., Mayor, M., & Monteiro, M. J. P. F. G. 2007, *A&A*, 469, 783 <http://dx.doi.org/10.1051/0004-6361:20077288>
- Sousa, S. G., Santos, N. C., Mayor, M., et al. 2008, *A&A*, 487, 373 <http://dx.doi.org/10.1051/0004-6361:200809698>
- Sousa, S. G., Alapini, A., Israelian, G., & Santos, N. C. 2010, *A&A*, 512, A13 <http://dx.doi.org/10.1051/0004-6361/200913388>
- Sousa, S. G., Santos, N. C., & Israelian, G. 2012, *A&A*, 544, A122 <http://dx.doi.org/10.1051/0004-6361/201219260>
- Sousa, S., 2014, arXiv:1407.5817 <http://adsabs.harvard.edu/abs/2014arXiv1407.5817S>
- Teixeira, G. D. C. et al. 2014, *in preparation*
- Tsantaki, M., Sousa, S. G., Adibekyan, V. Z., et al. 2013, *A&A*, 555, A150 <http://dx.doi.org/10.1051/0004-6361/201321103>
- Tsantaki, M., Sousa, S. G., Santos, N. C., Montalto, M., Delgado-Mena, E., Mortier, A., Adibekyan, V. Z., Israelian, G. 2014, ArXiv e-prints, 1407.6765 <http://adsabs.harvard.edu/abs/2014arXiv1407.6765T>
- Upton, G., Cook, I. 1996, *Understanding Statistics*. Oxford University Press.



Valenti, J. A., Piskunov, N. 1996, A&AS, 118 <http://adsabs.harvard.edu/abs/1996A%26AS..118..595V>